Stony Brook University

Spectroscopic and Mass Spectrometric Studies of Atmospherically Relevant Clusters

A Thesis Presented

by

Eleanor Castracane

to

The Graduate School

in Partial Fulfillment of the

Requirements

for the Degree of

Master of Science

in

Chemistry

Stony Brook University

May 2017

Stony Brook University

The Graduate School

Eleanor Castracane

We, the thesis committee for the above candidate for the

Master of Science degree, hereby recommend

acceptance of this thesis.

Christopher J. Johnson – Thesis Advisor
Assistant Professor, Department of Chemistry

Katherine B. Aubrecht – Thesis Committee Chair
Associate Professor, Department of Chemistry

Trevor J. Sears – Third Member of the Thesis Committee
Professor, Department of Chemistry

This thesis is accepted by the Graduate School.

Charles Taber
Dean of the Graduate School

Abstract of the Thesis

Spectroscopic and Mass Spectrometric Studies of Atmospherically Relevant Clusters

by

Eleanor Castracane

Master of Science

in

Chemistry

Stony Brook University

2017

The largest source of uncertainty in current climate models is found in the contribution of aerosol particles, which have both cooling and warming effects. Of this uncertainty, a significant fraction is due to an incomplete understanding of new particle formation, in which aerosols are formed directly from atmospheric trace vapor. Advances will require the development of a mechanistic framework describing the structures and thermodynamics of growth. Cluster size and composition can often be determined from fieldwork, but laboratory work must be done to determine energetics and structure. A major current focus of studies on new particle formation involves clusters of sulfuric acid and ammonia, and exchange of ammonia for amines. This work presents studies laying the groundwork for the development of a mechanism describing ammonia-amine exchange.

Clusters containing sulfuric acid and ammonia – both cationic and anionic – were formed via electrospray ionization, and cluster composition patterns were investigated through mass spectrometry. A major goal was to develop a rational approach to synthesizing clusters with specific compositions. Methylamine, dimethylamine, and trimethylamine can be straightforwardly substituted into the clusters. Structures of small cationic clusters of these compositions were investigated using cryogenic ion vibrational predissociation spectroscopy experiments to determine structural trends.

It is not enough to just be able to elucidate the structures of these clusters. Reactions occur in the atmosphere, and it would be useful to model those as well through thermochemistry. Temperature-controlled ion traps are being constructed to carry out these thermochemical measurements. Temperature could be a major source of uncertainty in these measurements, so experiments to determine the effective temperature of the ions in relation to the temperature of the trap were begun. Current work uses a cryogenic trap (~3.5 – 300K) and the ammonium-water binary system as a model. In these experiments, the temperature of the ion trap was varied and the temperature of the ions was determined by fitting the rovibrational features of the nearly-free water rotor. Results show that the derived temperature does indeed respond to changes in trap temperature, but that several challenges remain.

To nasty women everywhere.

Table of Contents

List of Figures

List of Tables

List of Abbreviations

CID – Collision-induced Decay

CIVP – Cryogenic Ion Vibrational Predissociation

CLOUD – Cosmics Leaving Outdoor Droplets

DFG – Difference Frequency Generation

DMA – Dimethylamine

IRMPD – Infrared Multi-photon Dissociation

MA – Methylamine

KTP – Potassium Tianyl Phosphate

KTA – Potassium Tianyl Arsenate

m/z – Mass-to-Charge Ratio

Nd:YAG – Neodymium-doped Yttrium Aluminum Garnet

OPA – Oscillating Parametric Amplifier

OPO – Oscillating Parametric Oscillator

RF – Radiofrequency

TMA – Trimethylamine

TOF – Time of Flight

Acknowledgements

First I must thank Dr. Susan Oatis. Without her keen eye and attention, I would have never considered studying physical chemistry.

My advisor, Chris Johnson, has been nothing short of incredible, always having faith in us and knowing exactly how to make us excited about everything. His high expectations and his determination to see his students succeed have been the source of the crash course in gaseous ion spectroscopy I have been given. I can only hope to one day master patience in the same manner as our postdoc, Sarah Waller, who has never once showed a hint of frustration at our repetitive questions. A lab is nothing without its students, and I have had the fortune to work with and learn from an amazing bunch: graduate students Emily Racow, Yi Yang, and John Kreinbihl; and undergraduates Pengyan Liu, Christina Kmiotek, and Kathy Nickson.

I am also appreciative of the guidance, motivation, and support I have received from many of the department's faculty members throughout my time at Stony Brook, especially from Kate Aubrecht, Andreas Mayr, Trevor Sears, and Eric Patterson.

Finally, I am grateful for the incredible friends I have: from the chemistry department, particularly Matt Hannigan, Katie Maffucci, Rebecca Koelln, and Tyger Salters, for helping me navigate all the ups and downs of the start of my graduate career; Hannah Mieczkowski, for getting dinner with me every single day leading up to the submission of this thesis; and Amanda Burke, for helping me justify poor decisions.

Chapter 1. Introduction

Aerosols are solid or liquid particles suspended in a gas, such as air. In our atmosphere, these aerosols can come from the anthroposphere: for example, from fossil fuel burning or dust ejected from mining; or from the biosphere, from places such as oceans, deserts, or forests. Aerosols are the largest source of error in climate change calculations, as they have both warming and cooling effects.[1] Alongside their effects on climate and cloud formation, aerosols also have impacts on human health and the breathability of air.[2]

Atmospheric new particle formation is a process of particular interest to many climate scientists, as it is not well understood but represents a large fraction of total aerosols.[1] Initially, aerosols are less than 3 nm in diameter, but they are able to grow to cloud condensation sizes (~100 – 400 nm)[1] if enough condensable vapors are around.[3,4]

"Atmospherically relevant" particles are aerosols that are believed to be common in cluster and cloud condensation nuclei formation. Sulfuric acid is widely believed to be the precursor for many new particle formation events,[5-7] and largely comes from the anthroposphere. Other precursors of interest include organic acids, amines, and diamines, which come from the biosphere; and ammonia, which can come from both natural and man-made sources.

Through field measurements, approximate size distributions can be surveyed, but for aerosols larger than 3mm, it is difficult to tell chemical composition.[8,9] To study chemical composition, aerosols can be formed in the Cosmics Leaving Outdoor Droplets (CLOUD) chamber at CERN. CLOUD is the first high-performing low-contaminant experiment drawn

[1] References for this chapter can be found on page 3.

to study aerosol nucleation and growth. It is a large, 26 m^3 steel drum containing a finely tuned atmosphere, in which rates of formation of aerosol clusters and their interactions with cosmic rays are studied.[10] Although many studies have been done on both chemical composition and growth of aerosols, the relationship between composition and cluster growth is not yet well known. Other areas of particular interest regarding atmospherically relevant aerosols are structure determination of aerosol clusters and acid/base interactions,[11] as acid/base interactions in minimally solvated environments are not well understood.

There are three ways that our lab currently studies ion clusters: mass spectrometry, Cryogenic Ion Vibrational Predissociation (CIVP), and Infrared Multi-photon Dissociation (IRMPD). Mass spectrometry is used for determining the composition of the clusters, whereas infrared spectroscopy helps to elucidate the structure.

It will also be necessary to study the thermochemistry of growth in the gas phase. To do this, we are constructing temperature-controlled ion traps to study temperature's effect on cluster structure and composition. These experiments reveal heats of formation and reaction barriers by modeling dissociation kinetics at given temperature and pressure, and can be used to determine the energetics of dissociation. Thus, assuming microscopic reversibility, the energetics governing growth can be determined on a structure-by-structure basis.

This thesis explores two instrumentational aspects of studying new particle formation: cluster formation through electrospray ionization (ESI), and ion cooling through CIVP. This thesis also explores steps towards structure determination of anionic ammonia-sulfuric acid aerosol clusters.

References

1. Boucher, O.; et al. Clouds and Aerosols. *Climate Change 2013: The Physical Science Basis. Contribution of Working Group I to the Fifth Assessment Report of the Intergovernmental Panel on Climate Change.* **2013**, 597, 622.
2. Forster, P.; et al. Changes in Atmospheric Constituents and in Radiative Forcing. *Climate Change 2007: The Physical Science Basis. Contribution of Working Group I to the Fourth Assessment Report of the Intergovernmental Panel on Climate Change.* **2007**, 135 – 136, 153 – 171.
3. Lihavainen, H.; et al. Production of "potential" cloud condensation nuclei associated with atmospheric new-particle formation in northern Finland. *J. Geophys. Res.* **2003**, *108*, 4782.
4. Yu, F.; Guo, L. Simulation of particle size distribution with a global aerosol model: contribution of nucleation to aerosol and CCN number concentrations. *Atmos. Chem. Phys.* **2009**, *9*, 7691 – 7710.
5. Kumala, M.; Lehtinen, K. E. J.; Laaksonen, A. Cluster activation theory as an explanation of the linear dependence between formation rate of 3 nm particles and sulphuric acid concentration. *Atmos. Chem. Phys.* **2006**, *6*, 787 – 793.
6. Kuang, C.; McMurry, P. H.; McCormick, A. V.; Eisele, F. L. Dependence of nucleation rates on sulfuric acid vapor concentration in diverse atmospheric locations. *J. Geophys. Res.* **2008**, *113*, D10209.
7. Spilä, M.; et al. The Role of Sulfuric Acid in Atmosheric Nucleation. *Science*. **2010**, *327*, 1243 – 1246.

8. Weber, R. J.; McMurry, P. H.; Eisele, F. L.; Tanner, D. J. Measurement of Expected Nucleation Precursor Species and 3 – 500 nm Diameter Particles at Mauna Loa Observatory, Hawaii. *J. Atmos. Sci.* **1995**, *52*, 2242 – 2257.

9. Ball, S. M.; Hanson, D. R.; Eisele, F. L.; McMurry, P. H. Laboratory studies of particle nucleation: Initial results for H_2SO_4, H_2O, and NH_3 vapors. *J. Geophys. Res.* **1999**, *104*, 23709 – 23718.

10. The CLOUD project | Welcome to CLOUD. http://cloud.web.cern.ch/cloud (Accessed 3 April 2017).

11. Bianchi, F.; et al. Insight into Acid-Base Nucleation Experiments by Comparison of the Chemical Composition of Positive, Negative, and Neutral Clusters. *Environ. Sci. Technol.* **2014**, *48*, 13675 – 13684.

Chapter 2. Descriptions of the Instruments

2.1 Action Spectroscopy

Absorbance spectroscopy measures the amount of light absorbed at a particular wavelength. Action spectroscopy, however, compares the wavelength of light used to its effectiveness in promoting a reaction. This was first seen in chlorophyll, where aerobic bacteria was observed to colonize near chlorophyll that was exposed to red-orange and violet light, but not green or yellow light.[1] This revealed that chlorophyll only photosynthesized and produced oxygen when exposed to red-orange and violet light.

The action spectrum is sometimes used instead of the absorbance spectrum, as it provides a better understanding of what wavelengths of light are resonant with the internal states of a molecule, and not just a reduction in transmission due to scattering, for example. Action spectroscopy also allows spectra to be recorded for extremely dilute samples, conceivably down to single molecules in cases where detection efficiency of the action is high. This allows spectra directly analogous to common absorption spectra to be obtained for samples in molecular beams or mass spectrometers. In principle, the energy barrier of a reaction can also be determined from the action spectrum, if the number of photons needed to cause a reaction could be determined.

In our instrument, dissociation is observed through Cryogenic Ion Vibrational Predissociation (CIVP) and Infrared Multi-photon Dissociation (IRMPD). In CIVP, ion clusters are cryogenically cooled and an inert gas, most commonly helium or deuterium, is "tagged" onto the cluster. The gas molecule messenger tag is not bonded to the cluster, but rather is attached through physisorption.

[1] References for this chapter can be found on page 13.

Through absorption of a photon, the inert gas tag is dissociated. After interacting with photons, the ion clusters are directed into a detector, which correlates the clusters with their masses. The action spectrum reflects the fraction of clusters of a specific mass that have dissociated at any given wavenumber. At wavenumbers that are absorbed by the cluster, there will be more dissociation, and thus a larger intensity of the dissociation product from the mass of interest. The change in intensity can be plotted against the wavenumber, and this will result in the infrared rotational-vibrational action spectrum (Figure 2.1).

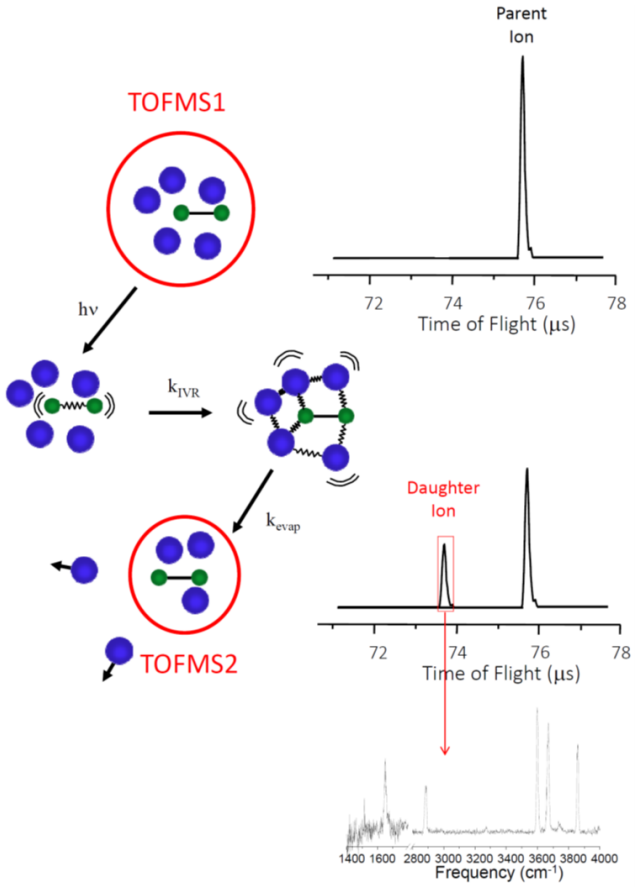

Figure 2.1 Depiction of the CIVP process. The molecule to be studied (green) is tagged with messenger tags (blue), which dissociate via interaction with a photon. The intensity of the daughter ion is recorded as tags dissociate, which leads to the ro-vibrational action spectrum.

IRMPD experiments are done very similarly, except there is no tagging in the cryogenic ion trap, and the dissociation is of the cluster into smaller molecular fragments after absorption of at least as many photons of a given wavenumber as the dissociation energy of the lowest-energy bond.

Limits arise for both CIVP and IRMPD. For CIVP, ions do not cool as expected and the observed temperature plateaus. Also, due to the need for an associated tag molecule, tag effects occur, and the rotational spectra can be affected through the strength of the associated bond. In IRMPD, there is no observable fingerprint region with the power available from conventional tabletop laser systems, and some broadening and red shifting of peaks is typically observed due to anharmonic coupling. Also, the relative intensities of peaks cannot be trusted because the cross-sections for absorption of more than one photon are likely to be different than those for the first photon.

2.2 Tandem Time-of-Flight Mass Spectrometer/Infrared Laser

The Johnson Lab has built a custom tandem electrospray ionization (ESI)/cryogenic ion trap/tandem Time-of-Flight (TOF) mass spectrometer and interfaced it with a tunable infrared optical parametric converter system pumped by a neodymium-doped yttrium aluminum garnet (Nd:YAG; Nd:$Y_3Al_5O_{12}$) laser (Figure 2.2).

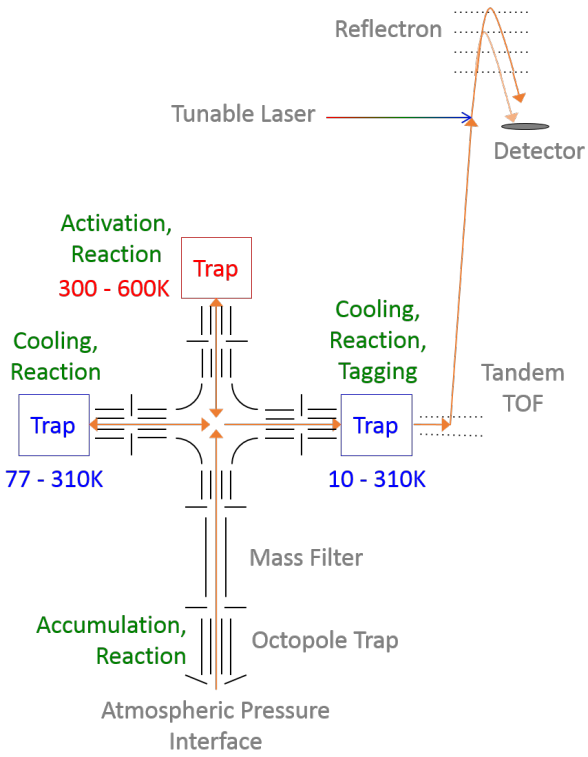

Figure 2.2 Cartoon depiction of the instrument.

Aerosol clusters are formed through electrospray ionization (ESI) of millimolar-concentrated solutions in a sealed, controlled atmosphere environment. In some cases, a reservoir containing amines of interest will be attached to the electrospray chamber, so that addition or substitution of molecules may occur in the gas phase. This region is sometimes held at a slight vacuum, which aids with gaseous substitution involving the liquid amines. The clusters are then directed to a cryogenic radiofrequency octopole ion trap (~3.5 to 300 K), where messenger tagging occurs.

These tagged clusters are orthogonally accelerated into a TOF tube using a Wiley-McLaren arrangement (Figure 2.3).[2] The ions are spatially focused between Plates 1 and 2. Plate 2, which has a fine mesh grid to allow ions to pass through, is grounded when ions enter the TOF region, and pulsed to +4000 volts once all the ions have left the ion trap. Plate 1, the source backing plate, is a solid plate, so ions cannot travel through it, and it is pulsed at

approximately +4340 volts once all ions have left the trap, to accelerate them past Plates 2 and 3, and down the TOF. Plate 3, which also has a mesh grid, is grounded to aid in focusing the ions.

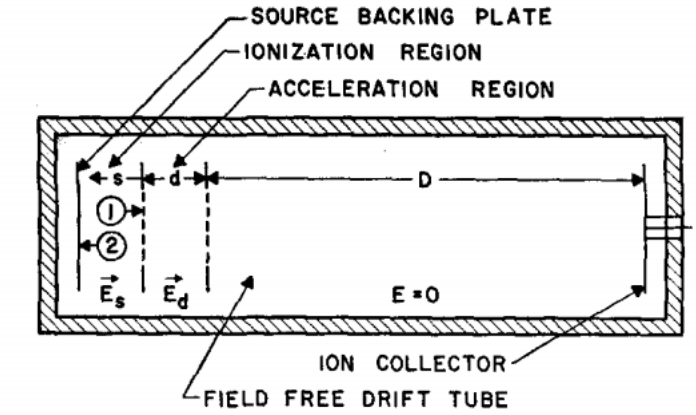

Figure 2.3 Depiction of the Wiley-McLaren plate arrangement.[2] In our instrument, we call the source backing plate Plate 1 and the middle plate Plate 2.

At the end of the TOF tube is a mass gate. If the clusters were previously tagged, the mass gate is used to filter out any untagged clusters, so that just the tagged clusters will meet with the laser. This is imperative, as the laser knocks off the tag, recreating (mass-wise) the original untagged cluster. The originally untagged clusters must be removed by the mass gate. The originally untagged clusters do not hold spectroscopic information that is important for our experiments, and it is difficult to differentiate between clusters that were never tagged and those that had their tags removed absorption. The timing for the mass gate is fine-tuned so that the untagged cluster is not allowed past the mass gate, but all higher masses, including the tagged cluster, are allowed.

An unseeded ~600 mJ at 1064 nm fundamental from a Nd:YAG pump laser (Continuum Surelite EX) is injected into an optical parametric oscillator/amplifier (OPO/OPA) system (LaserVision) to produce photons with energies from 600 cm^{-1} to 4500

cm^{-1}. For the sake of this work, "mid" infrared will be defined as 2400 cm^{-1} to 4500 cm^{-1} and "far" infrared will be 600 cm^{-1} to 2400 cm^{-1}. The LaserVision OPO/OPA system uses a set of six or seven nonlinear crystals to achieve desired energies.

Six crystals, made from potassium titanyl phosphate (KTP) and potassium titanyl arsenate (KTA), that are common to both mid and far IR move in pairs to phase match the pump wavelength with the two wavelengths produced by the nonlinear process. To reach far IR, an angle-tuned silver gallium selenide ($AgGaSe_2$) crystal is used in conjunction with the other crystals, in a process known as difference frequency generation (DFG).

In optical parametric oscillation, two nonlinear crystals are used to split a beam of light (the "pump") into a "signal" and an "idler", where the frequency of the signal is higher than the frequency of the idler. The idler is then sent into the OPA system. Optical parametric amplification happens when a "weak wave" (in our case, the OPO idler) and a "strong wave" (our pump beam) pass through two sets of two nonlinear crystals. The gain of the OPO idler is amplified, and this becomes the new OPA signal. The gain of the pump is reduced, and the third beam at the difference between the pump and signal photon energies becomes the new OPA idler. For mid IR, only the idler is used; the signal is filtered out, but both the signal and the idler are used for far IR. In DFG, idler coming from the OPA is subtracted from the signal coming from the OPA. The crystal positions are all calibrated in the LaserVision Motor Controls program from the manufacturer, which is used concurrently with our own lab-built LabView data acquisition program.

The laser intersects the ion beam after the mass gate, and is timed so that only the cluster of interest is irradiated. Depending on the experiment done, the laser either knocks off the tag or dissociates the untagged cluster, and the resulting lower-kinetic-energy ion

continues down the ion beam's path, until it is repelled by the reflectron into a detector. The reflectron temporally separates the tagged and dissociated clusters by energy, which is necessary because they have the same lab-frame velocity, so that they arrive at different times at the detector.

2.3 Thermo-Fisher LTQ Mass Spectrometer

Another tool used in these studies is a Thermo-Fisher LTQ mass spectrometer. The LTQ has a two-dimensional linear quadrupole ion trap mass analyzer. The LTQ can work with many types of ion sources, but currently, ions are only formed with an ESI source. As opposed to the TOF instrument, the source chamber of the LTQ is at open to the atmosphere, and the capillary from which solution is sprayed is held above 250°C.

Ion optics include three sets of linear quadrupoles and lenses that accelerate ions down into the mass analyzer. The mass analyzer consists of a single, linear two-dimensional quadrupole ion trap. Helium is used as a damping gas in the trap to slow down the incoming ions so that they may be trapped inside the radiofrequency (RF) field. The ion trap is split into three sections, and ions are ejected through a slit made in one of the poles of the middle section. Having three sections limits possible fringe distortions that would hinder ion entrance into the trap. It also allows for different DC biases on each section, creating a potential well in which the ions can gather.[3] The ion detection system in the LTQ has two off-axis dynode detectors. This produces a high signal-to-noise ratio, as the detectors are outside of the ion beam, and it allows for easy enabling of polarity switching.

The LTQ is capable of performing MS^n experiments through collision-induced dissociation (CID), nominally to any number *n*, as long as ions exist. This type of tandem

mass spectrometry is done in time, rather than in space. The ions are trapped and dissociated in the same quadrupole ion trap, using the buffer gas as the CID gas.[4] This technique is useful in determining cluster composition, as the cluster can easily be fragmented into its constituents. It can also provide qualitative information on the ordering of binding energies of the cluster constituents, since the weakest-binding components will dissociate at low collision intensities whereas more strongly bound species require higher activation. Since the dissociation occurs within the same trap as the ions are trapped in, tandem mass spectrometry can occur multiple times, and is not limited to the number of traps available, as is tandem in space mass spectrometry.

References

1. Engelmann, T. W. Ein Beitrag zur vergleichenden Physiologie des Licht- und Farbensinnes. *Pflüg. Arch. Eur. J. Phys*. **1883**, *30*, 95–124.

2. Wiley, W. C.; McLaren, I. H. Time-of-Flight Mass Spectrometer with Improved Resolution. *The Review of Scientific Instruments*. **1955**, *26*, 1150–1157.

3. Schwartz, J.C.; Senko, M. W.; Skyla, J. E. P. A Two-Dimensional Quadrupole Ion Trap Mass Spectrometer. *J. Am. Soc. Mass Spectrom.* **2002**, *13*, 659–669.

4. Johnson, J. V.; Yost, R. A.; Kelley, P. E; Bradford, D. C. Tandem-in-Space and Tandem-in-Time Mass Spectrometry: Triple Quadrupoles and Quadrupole Ion Traps. *Anal. Chem.* **1990**, *62*, 2162-2172.

Chapter 3. Effective Temperature of Trapped Ions

3.1 Introduction

In the quest to further our understanding of our atmosphere, we must be able to measure the energetics of the reactions underlying new particle formation. Temperature-controlled ion traps can be used for this purpose and are currently being built for incorporation into the instrument, but temperature can still be a source of uncertainty that leads to inaccuracy of thermochemical measurements. Therefore, we must be able to determine how the effective temperature of the ions corresponds to the trap temperature.

Cooling of ions in a RF ion trap on a reasonable time scale occurs through inelastic collisions with cold buffer gas (typically helium). It is expected that when cooling an ion, it will thermally equilibrate to the temperature of the buffer gas in which it resides. However, it is not clear that this is the case – previously, ions have been observed to cool much slower than the buffer gas does below a certain temperature (Figure 3.1).[1] It is likely that heating processes, such as the strong driving forces from RF voltages required to trap ions, may yield an equilibrium temperature necessarily higher than the trap or buffer gas temperatures.

[1] References for this chapter can be found on page 21.

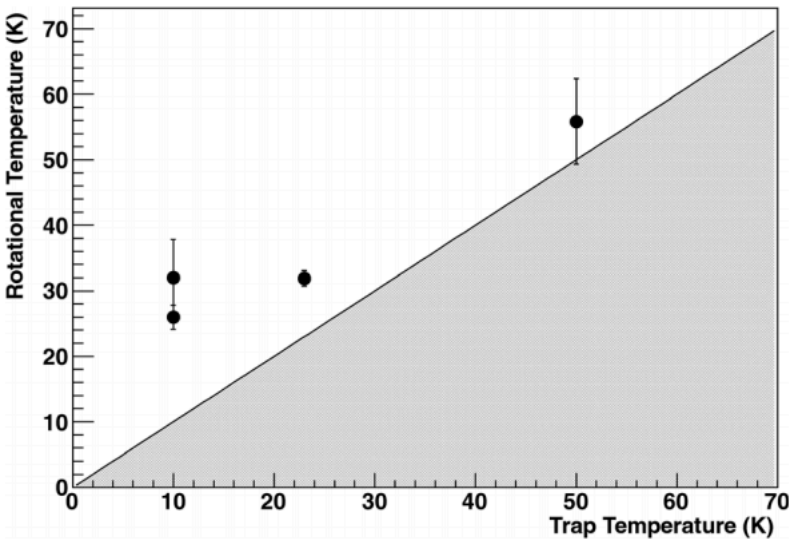

Figure 3.1 Observed rotational temperatures for OH^- anions at various trap temperatures.[1]

In order to estimate the temperature at which deviations may occur, an experiment with an observable that depends on temperature is required, and a "probe" molecule must be selected. A rotationally resolved vibrational spectrum is a convenient temperature gauge, but the probe molecule must meet several criteria:

1. The rotational constant is large enough that it can be resolved within the 3-to-5 wavenumber resolution of our laser;
2. The temperature to reach the next *J*-value is low enough that it can easily be populated; and
3. We can easily record a linear spectrum of the molecule.

We decided to use the ammonium-water complex as our probe molecule. Water's rotational constant in this complex is 14 cm^{-1}, large enough that even with a messenger tag, the rotational spectrum can be resolved by our laser.

Both IRMPD and CIVP have their pros and cons as experimental methods. For CIVP, we only need to use one photon to knock off the tags, so the relative intensities of the peaks

ought to be correct. The downside of messenger tagging is that the presence of a tag changes the structure slightly as a function of the tag's binding energy, and the tags are heavily temperature dependent. Messenger tags are temperature dependent in that only certain tags can bind at certain temperatures (Table 1.3). This means that the tag gas must be changed as the temperature range changes.

Table 3.1 Approximate tagging temperatures for various messenger tags.

Tag	**Appx. Tagging Temperature**
He	< 5K
D_2	12 – 17K
N_2	20 – 50K
CO_2	80 – 120K

IRMPD, however, does not need a messenger tag, so it can be performed at any temperature. Unfortunately, the relative intensities of the peaks in the spectrum may not be quantitatively accurate, since we do not know what the absorption cross-section is for the second and higher photons. This means there is an inherent uncertainty in even the relative intensities of the peaks, which is reflected as an uncertainty in fitting to a Boltzmann distribution to retrieve a temperature.

Regardless, we will use both methods to see which will be more accurate. It is naïvely expected that the CIVP spectra should appear colder than the IRMPD spectra, because tagging by definition must occur for cold ions. The upper temperature limit to messenger tagging is set by the binding energy of the tag. Ions that are hotter than the maximum binding energy will not tag, since the tag will desorb from the ion. As a result, CIVP can be expected to only occur for a colder population of ions that exist within the confines of the tag's binding energy limits, whereas IRMPD can occur for any molecule at any temperature.

Temperature is just the population distribution among states, and the populations should follow a Boltzmann distribution. Any features we see in the rotational spectrum depend on the innate strength of the transition and the percent of molecules that exist in that state, the latter being very important in defining temperature. In order to determine temperature from these spectra, we must make two assumptions: the relative intensities are, in fact, good approximations of the population that exist in that state; and that the clusters are in thermal equilibrium with the surrounding buffer gas in the trap.

3.2 Experimental Work

The ammonium-water cluster was formed by electrospraying 1 mM $(NH_4)_2SO_4$ solution containing 0.1% formic acid in a 50:50 water:methanol mixture. We recorded IRMPD spectra at multiple ion trap temperatures: 4K, 13.5K, 17K, 20K, and 25K. We attempted to helium and deuterium tag the ammonium-water cluster at these temperatures for CIVP, but were only able to helium tag at 4K and deuterium tag at 13.5K and 17K. All CIVP spectra were recorded with two tags.

Expected rotational spectra were calculated and fitted to experimental spectra in PGOPHER using rotational constants calculated at the MP2/aug-cc-pVTZ level of theory as implemented in the Gaussian 09 suite of programs.[2] This procedure is complex due to the fact that the water and ammonia are nearly free internal rotors, increasing the number of dimensions of the problem from the typical three rotations to four. A reduced-dimensionality procedure has been developed for preliminary analysis of the spectrum, in which the ammonia rotor is ignored, leaving only two rotations of the full cluster and one of just the water.[3] The doubly-tagged ammonium-water cluster is an asymmetric top. The rotational

constants A = 0.12 cm^{-1}, B = 14 cm^{-1}, and C = 0.087 cm^{-1} were calculated for the helium-tagged rotor, and A = 0.13 cm^{-1}, B = 14 cm^{-1}, and C = 0.099 cm^{-1} were calculated for the deuterium-tagged rotor. The nuclear spin weights for the ammonium-water cluster must take into account ortho/para water, ideally giving rise to a 3:1 intensity fluctuation for odd and even rotational states.

Trying to fit our spectra in PGOHPER proved to be much more difficult than we expected. For CIVP at 13.5K (Figure 3.2), the nuclear spin weights of 9:4 allowed the expected spectra to converge to our experimental spectra, but these weights did not work for CIVP at 4K (Figure 3.3). Using weights of 11:2 worked instead, a result that is not currently understood. It is not unreasonable to think that the spin statistics may not be the canonical 3:1 in the cluster due to broken symmetry caused by the ammonia molecule and the tag, so for now the spin weights are treated as a fitting variable.

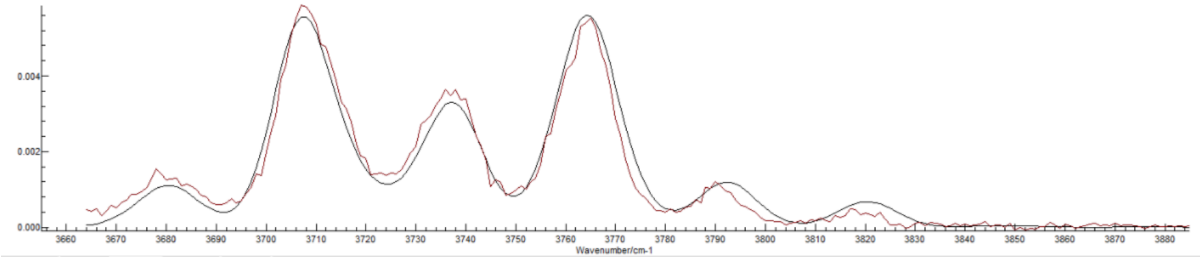

Figure 3.2 PGOPHER fit for 13.5K CIVP spectrum. The CIVP spectrum is red, and the PGOPHER fit is black.

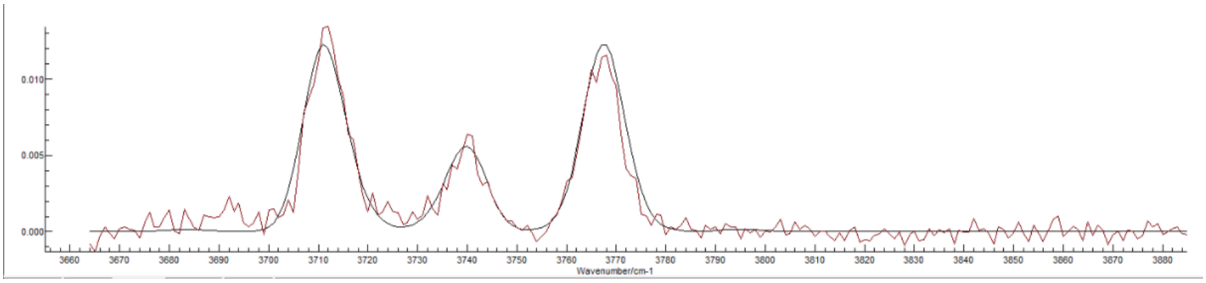

Figure 3.3 PGOPHER fit for 4K CIVP spectrum. The CIVP spectrum is red, and the PGOPHER fit is black.

PGOPHER estimates the effective temperature of our ions at 13.5K to be 73.7±5.2K, and the effective temperature of our ions at 4K to be 22.5±2.1K. This is consistent with the findings of Wester's group, in which ion temperatures were significantly higher than the trap temperatures, though the 4 K measurement here is somewhat lower than their result at 10 K.

For reasons beyond our current understanding, we were unable to get a fit for the CIVP spectrum at 17K to converge.

IRMPD spectra at each temperature (Figure 3.4) appear to all be very similar, and much colder than they should be (Table 3.2). It is possible that the two-photon IRMPD process does not produce reasonable relative intensities, even for bands in a single rovibrational manifold.

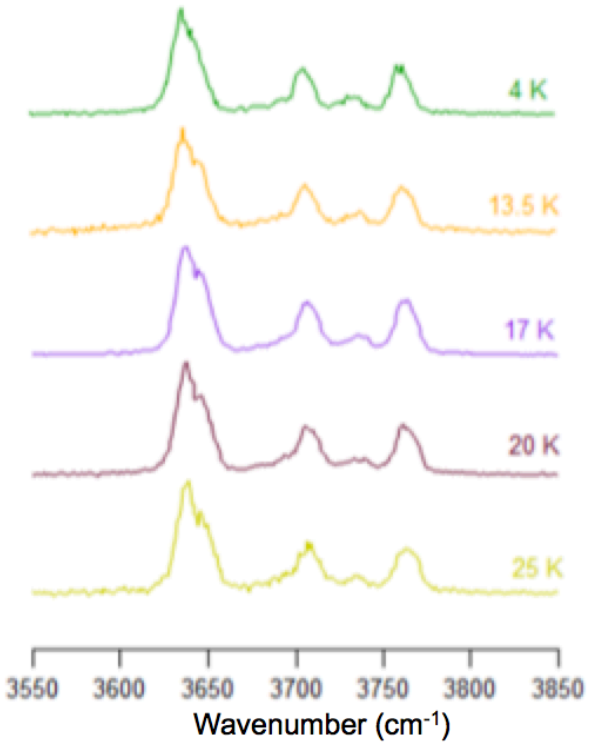

Figure 3.4 IRMPD spectra at various temperatures. The OH asymmetric stretch does not appear to change with increasing temperature.

Table 3.2 PGOPHER fits for IRMPD spectra at various temperatures.

Ion Trap Temperature	Rotational Temperature
4K	16.1±1.4K
13.5K	15.8±1.4K
17K	17.7±1.4K
20K	19.9±2.1K
25K	21.1±2.8 K

3.3 Future Work

The determination of temperature is not as straightforward as we had initially thought. The basic trends for CIVP are qualitatively expected, but we need to be able to better quantitatively interpret our spectra. Ion temperature is likely to depend on more than just the trap temperature – the trap voltages may also need to be taken into account, and it may be possible to dramatically lower the temperature by optimizing these settings. Ions can reheat through collisions with each other and the buffer gas, and can also be affected by the amplitude of the RF signal used to trap them. We would like to be able to reduce any other sources of uncertainty in temperature, so the best approach is likely to find conditions to tag helium onto the ammonium-water cluster (since this is the weakest tag and thus likely to be the coldest conditions), and without changing any trap conditions other than temperature, increase the temperature until we can deuterium tag.

It seems that IRMPD is not reliable for the lower temperatures that we have studied, but we would like to confirm its unreliability by studying significantly higher temperatures' effects on the IRMPD spectrum.

References

1. Otto, R.; von Zastrow, A.;Best, T.; Wester, R. Internal state thermometry of cold trapped molecular anions. *Phys. Chem. Chem. Phys.* **2013**, *15*, 612 – 618.

2. Frisch, M.J.; et al. Gaussian 09, Revision A.02, Gaussian, Inc., Wallingford CT, 2016.

3. Pankewitz, T.; et al. Infrared spectrum of $NH_4^+(H_2O)$: Evidence for mode specific fragmentation. *J. Chem. Phys.* **2007**, *126*, 074307.

Chapter 4. Formation and Structure Elucidation of Ammonium Bisulfate Clusters

4.1 Introduction

Sulfuric acid and ammonia are commonly found in aerosols.[1-3] Sulfuric acid has been found to be a major driving force in atmospheric new particle formation.[3,4] Both ammonia and sulfuric acid are found in high concentrations as trace gases in the atmosphere, as a result of pollution and natural processes.[5] It is currently hypothesized that new particles are stabilized by salt-bridge formation between ammonia and sulfuric acid, and that further stabilization is achieved by exchange of more basic amines for ammonia.[6] For the spectroscopy experiments to be relevant, it is important to study clusters with compositions closely matching those expected to be found in the atmosphere. This requires a higher level of sophistication in our capabilities to synthesize specific cluster compositions. In our lab, clusters of ammonia and sulfuric acid can be formed by electrospraying dilute solutions of ammonium sulfate or ammonium bisulfate. Amine exchange can be achieved by either adding amines to the ESI solution, or by adding amine vapor to the atmosphere surrounding the ESI emitter.

Our group has extensively studied the structure and growth of cationic ammonium bisulfate clusters. It is critical for the composition of these clusters to closely match those expected to be found in the atmosphere. To study cationic clusters, we use a 1mM $(NH_4)_2SO_4$ in 50:50 water:methanol 0.1% formic acid solution. We see both singly and doubly charged clusters (Figure 4.1), which follow a pattern: they contain ammonium, ammonia, and sulfuric acid. The naming scheme is (*m,n*), for $(NH_4^+)_m(HSO_4^-)_n$, where m is typically n+1 for singly charged clusters or n+2 for doubly-charged ones.

[1] References for this chapter can be found on page 34.

We studied methylamine (MA), dimethylamine (DMA), and trimethylamine (TMA) substitution primarily for the (2,1) and (3,2) clusters. Amine substitution can occur by adding the amine into the electrospray solution for methylamine and dimethylamine, or by including it in the controlled electrospray atmosphere for dimethylamine and trimethylamine (Figure 4.2). The naming scheme for substituted clusters is (*l,m,n*), where *l* is the number of amines substituted in, and *m* and *n* are the same as above.

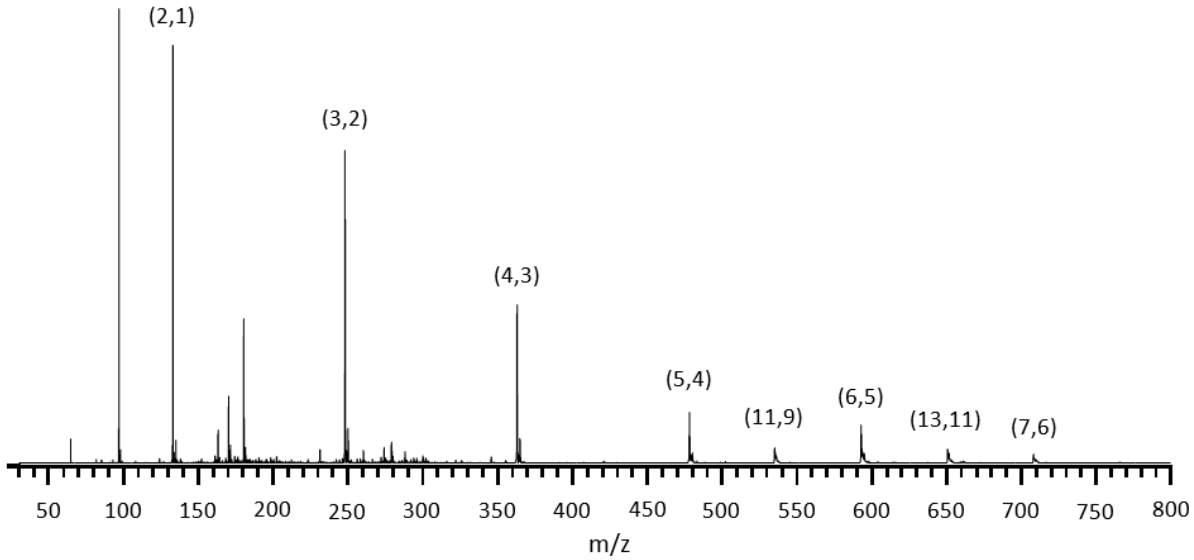

Figure 4.1 Mass spectrum of cationic $(NH_4)_2SO_4$ clusters. Doubly charged clusters begin to appear when $m = n+2 = 11$.

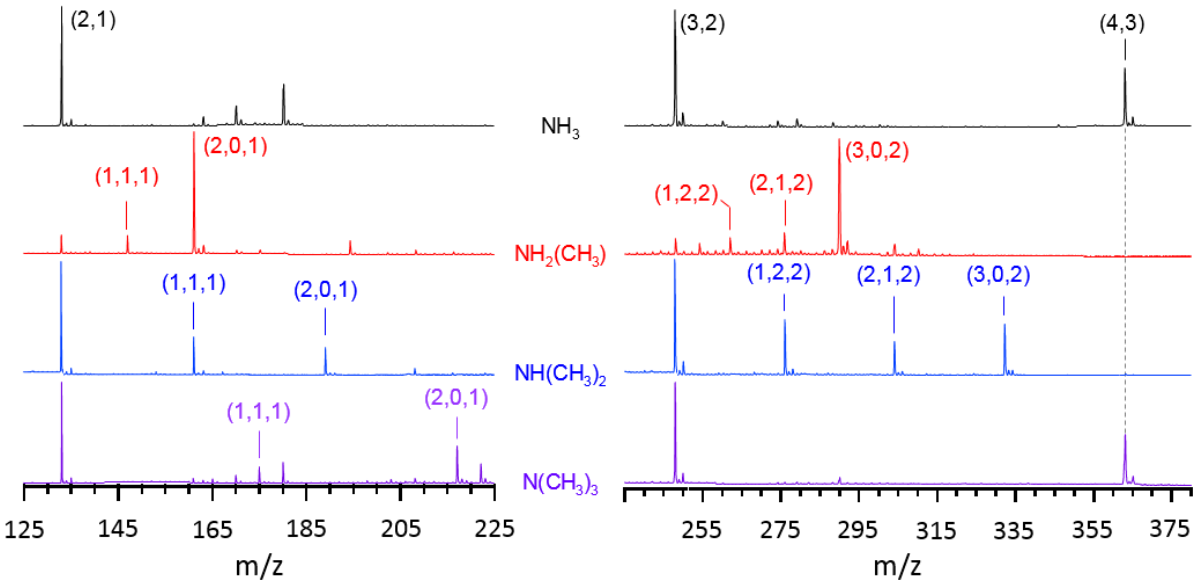

Figure 4.2 Comparison of amine substitution for the (2,1) and (3.2) clusters. Here, the amines were integrated into the electrospray solution, which (as in TMA for (3,2)) does not always work.

We also conducted mid and far IR CIVP experiments (doubly deuterium tagged) of the (2,1) and (3,2) unsubstituted and fully substituted clusters (SI 4.1, 4.2). The lack of NH stretches in the spectra with increased alkyl amine substitution is consistent with the expected loss of free NH moieties, as NH_4^+ is replaced with $NH_2(CH_3)_2^+$ or $NH(CH_3)_3^+$.

4.2 Experimental Work

To form negatively charged clusters through ESI, we find that the solution has to be more concentrated than solutions for positive clusters.[7] We also find that ammonium sulfate solutions form clusters more readily than ammonium bisulfate solutions, so ammonium sulfate solutions of varying concentrations were screened on the LTQ XL mass spectrometer. Aqueous ammonium sulfate solutions of 1 mM, 5 mM, and 10 mM concentrations with 0.1% ammonium hydroxide were introduced into the LTQ mass spectrometer, and their mass

spectra were recorded (Figure 4.3). The 1 mM solution was more congested at lower m/z, and less intense than 5 or 10 mM solutions, which had very similar mass spectra.

Unfortunately, with increasing concentration comes increased instability in the electrospray. Oftentimes, instead of being sprayed, the solution forms a liquid bead on the tip of the electrospray emitter, until it gets too large (or is otherwise knocked off the tip) and then gets sucked in. This process causes a dip in the electrospray current every time the bead is forming, which is indicative of a non-continuous introduction of ions into the instrument. Due to this, the 5 mM solution was used instead of the 10 mM solution, even though their mass spectra were similar.

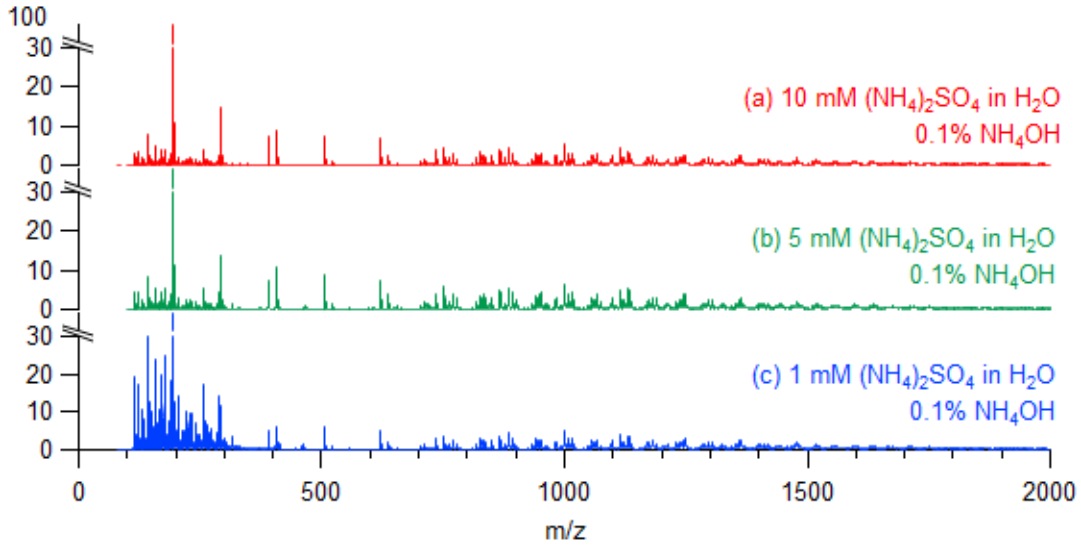

Figure 4.3 Various concentrations of aqueous $(NH_4)_2SO_4$ solutions used on the LTQ. (a) 10 mM $(NH_4)_2SO_4$; 0.1% NH_4OH (b) 5 mM $(NH_4)_2SO_4$; 0.1% NH_4OH (c) 1 mM $(NH_4)_2SO_4$; 0.1% NH_4OH

Collision-induced dissociation (CID) experiments were performed on some of the high intensity, low m/z peaks (SI 4.3 – 4.8). The CID experiments suggest that these clusters begin with a bisulfate anion, and have neutral sulfuric acid and ammonia incorporated. However, they are not able to report on the degree of proton transfer, or salt bridge formation within the cluster, which can instead be probed spectroscopically.

The aqueous 5 mM $(NH_4)_2SO_4$ solution with 0.1% NH_4OH was introduced into the TOF instrument. Clusters were formed, but not in as great numbers as on the LTQ (Figure 4.4a). This may be due to the solution being only aqueous – many times, a solvent mixture is used,[7] as was in our positive clusters. A 1:1 5 mM $(NH_4)_2SO_4$ in water/0.1% NH_4OH:methanol solution was mixed in the syringe used for solution introduction (Figure 4.4b). The mass spectra were calibrated in mMass[8] using a reference library containing exact cluster masses (SI 4.9).

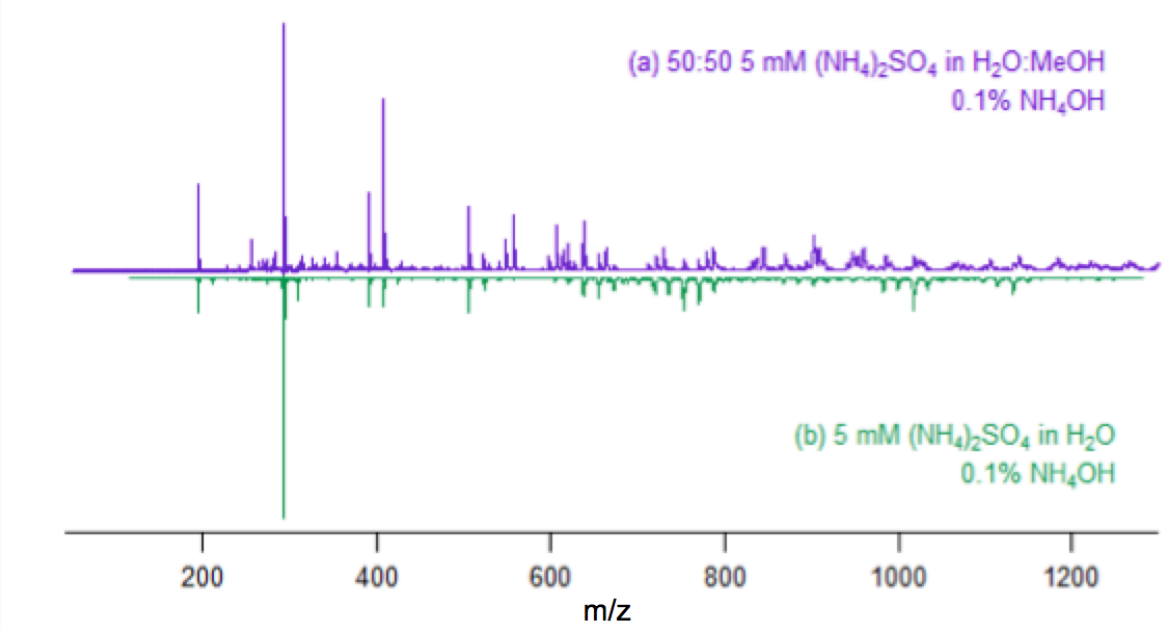

Figure 4.4 Comparison between aqueous and water/methanol solutions on the TOF. The water/methanol mixture (a) shows more intense peaks than the aqueous solution (b).

Two charts were used to visualize the clusters that were formed, and to see if any pattern emerges: one for singly charged species (Table 4.1), and one for doubly charged species (Table 4.2). The tables are labeled across the top for increasing ammonia presence and down the side for increasing sulfuric acid presence. The numbering scheme we used for cationic clusters was adapted for the anionic clusters, but with one difference: the bisulfate charge carrier is included in the sulfuric acid count. So, the first entry at (0,1) indicates no

ammonia or sulfuric acid – just the mass-to-charge ratio of the charge carrier. The entry at (1,1) indicates the mass-to-charge ratio of one ammonia and no sulfuric acid on the charge carrier, and its transpose (0,2) indicates the mass-to-charge ratio one sulfuric acid and no ammonia on the charge carrier.

Table 4.1 Chart of masses for singly charged species. The first entry (0,1) represents the charge carrier for this chart: a single bisulfate anion. Across a row represents more ammonia addition; down a column represents more sulfuric acid addition.

	0	1	2	3	4	5	6	7	8	9	10	11	12	13	14	15	16	17	18	19	20	21	22	23	24
1	97	114	131	148	165	182	199	216	233	250	267	284	301	318	335	352	369	386	403	420	437	454	471	488	505
2	195	212	229	246	263	280	297	314	331	348	365	382	399	416	433	450	467	484	501	518	535	552	569	586	603
3	293	310	327	344	361	378	395	412	429	446	463	480	497	514	531	548	565	582	599	616	633	650	667	684	701
4	391	408	425	442	459	476	493	510	527	544	561	578	595	612	629	646	663	680	697	714	731	748	765	782	799
5	489	506	523	540	557	574	591	608	625	642	659	676	693	710	727	744	761	778	795	812	829	846	863	880	897
6	587	604	621	638	655	672	689	706	723	740	757	774	791	808	825	842	859	876	893	910	927	944	961	978	995
7	685	702	719	736	753	770	787	804	821	838	855	872	889	906	923	940	957	974	991	1008	1025	1042	1059	1076	1093
8	783	800	817	834	851	868	885	902	919	936	953	970	987	1004	1021	1038	1055	1072	1089	1106	1123	1140	1157	1174	1191
9	881	898	915	932	949	966	983	1000	1017	1034	1051	1068	1085	1102	1119	1136	1153	1170	1187	1204	1221	1238	1255	1272	1289
10	979	996	1013	1030	1047	1064	1081	1098	1115	1132	1149	1166	1183	1200	1217	1234	1251	1268	1285	1302	1319	1336	1353	1370	1387
11	1077	1094	1111	1128	1145	1162	1179	1196	1213	1230	1247	1264	1281	1298	1315	1332	1349	1366	1383	1400	1417	1434	1451	1468	1485
12	1175	1192	1209	1226	1243	1260	1277	1294	1311	1328	1345	1362	1379	1396	1413	1430	1447	1464	1481	1498	1515	1532	1549	1566	1583
13	1273	1290	1307	1324	1341	1358	1375	1392	1409	1426	1443	1460	1477	1494	1511	1528	1545	1562	1579	1596	1613	1630	1647	1664	1681
14	1371	1388	1405	1422	1439	1456	1473	1490	1507	1524	1541	1558	1575	1592	1609	1626	1643	1660	1677	1694	1711	1728	1745	1762	1779
15	1469	1486	1503	1520	1537	1554	1571	1588	1605	1622	1639	1656	1673	1690	1707	1724	1741	1758	1775	1792	1809	1826	1843	1860	1877
16	1567	1584	1601	1618	1635	1652	1669	1686	1703	1720	1737	1754	1771	1788	1805	1822	1839	1856	1873	1890	1907	1924	1941	1958	1975
17	1665	1682	1699	1716	1733	1750	1767	1784	1801	1818	1835	1852	1869	1886	1903	1920	1937	1954	1971	1988	2005	2022	2039	2056	2073
18	1763	1780	1797	1814	1831	1848	1865	1882	1899	1916	1933	1950	1967	1984	2001	2018	2035	2052	2069	2086	2103	2120	2137	2154	2171
19	1861	1878	1895	1912	1929	1946	1963	1980	1997	2014	2031	2048	2065	2082	2099	2116	2133	2150	2167	2184	2201	2218	2235	2252	2269
20	1959	1976	1993	2010	2027	2044	2061	2078	2095	2112	2129	2146	2163	2180	2197	2214	2231	2248	2265	2282	2299	2316	2333	2350	2367
21	2057	2074	2091	2108	2125	2142	2159	2176	2193	2210	2227	2244	2261	2278	2295	2312	2329	2346	2363	2380	2397	2414	2431	2448	2465
22	2155	2172	2189	2206	2223	2240	2257	2274	2291	2308	2325	2342	2359	2376	2393	2410	2427	2444	2461	2478	2495	2512	2529	2546	2563
23	2253	2270	2287	2304	2321	2338	2355	2372	2389	2406	2423	2440	2457	2474	2491	2508	2525	2542	2559	2576	2593	2610	2627	2644	2661
24	2351	2368	2385	2402	2419	2436	2453	2470	2487	2504	2521	2538	2555	2572	2589	2606	2623	2640	2657	2674	2691	2708	2725	2742	2759
25	2449	2466	2483	2500	2517	2534	2551	2568	2585	2602	2619	2636	2653	2670	2687	2704	2721	2738	2755	2772	2789	2806	2823	2840	2857

Table 4.2 Chart of masses for doubly charged species. The first entry (0,1) represents the charge carrier for this chart: two bisulfate anions. Across a row represents more ammonia addition; down a column represents more sulfuric acid addition. Every entry is divided by 2 for the mass-to-charge ratio of each cluster.

	0	1	2	3	4	5	6	7	8	9	10	11	12	13	14	15	16	17	18	19	20	21	22	23	24
1	97	105.5	114	122.5	131	139.5	148	156.5	165	173.5	182	190.5	199	207.5	216	224.5	233	241.5	250	258.5	267	275.5	284	292.5	301
2	146	154.5	163	171.5	180	188.5	197	205.5	214	222.5	231	239.5	248	256.5	265	273.5	282	290.5	299	307.5	316	324.5	333	341.5	350
3	195	203.5	212	220.5	229	237.5	246	254.5	263	271.5	280	288.5	297	305.5	314	322.5	331	339.5	348	356.5	365	373.5	382	390.5	399
4	244	252.5	261	269.5	278	286.5	295	303.5	312	320.5	329	337.5	346	354.5	363	371.5	380	388.5	397	405.5	414	422.5	431	439.5	448
5	293	301.5	310	318.5	327	335.5	344	352.5	361	369.5	378	386.5	395	403.5	412	420.5	429	437.5	446	454.5	463	471.5	480	488.5	497
6	342	350.5	359	367.5	376	384.5	393	401.5	410	418.5	427	435.5	444	452.5	461	469.5	478	486.5	495	503.5	512	520.5	529	537.5	546
7	391	399.5	408	416.5	425	433.5	442	450.5	459	467.5	476	484.5	493	501.5	510	518.5	527	535.5	544	552.5	561	569.5	578	586.5	595
8	440	448.5	457	465.5	474	482.5	491	499.5	508	516.5	525	533.5	542	550.5	559	567.5	576	584.5	593	601.5	610	618.5	627	635.5	644
9	489	497.5	506	514.5	523	531.5	540	548.5	557	565.5	574	582.5	591	599.5	608	616.5	625	633.5	642	650.5	659	667.5	676	684.5	693
10	538	546.5	555	563.5	572	580.5	589	597.5	606	614.5	623	631.5	640	648.5	657	665.5	674	682.5	691	699.5	708	716.5	725	733.5	742
11	587	595.5	604	612.5	621	629.5	638	646.5	655	663.5	672	680.5	689	697.5	706	714.5	723	731.5	740	748.5	757	765.5	774	782.5	791
12	636	644.5	653	661.5	670	678.5	687	695.5	704	712.5	721	729.5	738	746.5	755	763.5	772	780.5	789	797.5	806	814.5	823	831.5	840
13	685	693.5	702	710.5	719	727.5	736	744.5	753	761.5	770	778.5	787	795.5	804	812.5	821	829.5	838	846.5	855	863.5	872	880.5	889
14	734	742.5	751	759.5	768	776.5	785	793.5	802	810.5	819	827.5	836	844.5	853	861.5	870	878.5	887	895.5	904	912.5	921	929.5	938
15	783	791.5	800	808.5	817	825.5	834	842.5	851	859.5	868	876.5	885	893.5	902	910.5	919	927.5	936	944.5	953	961.5	970	978.5	987
16	832	840.5	849	857.5	866	874.5	883	891.5	900	908.5	917	925.5	934	942.5	951	959.5	968	976.5	985	993.5	1002	1010.5	1019	1027.5	1036
17	881	889.5	898	906.5	915	923.5	932	940.5	949	957.5	966	974.5	983	991.5	1000	1008.5	1017	1025.5	1034	1042.5	1051	1059.5	1068	1076.5	1085
18	930	938.5	947	955.5	964	972.5	981	989.5	998	1006.5	1015	1023.5	1032	1040.5	1049	1057.5	1066	1074.5	1083	1091.5	1100	1108.5	1117	1125.5	1134
19	979	987.5	996	1004.5	1013	1021.5	1030	1038.5	1047	1055.5	1064	1072.5	1081	1089.5	1098	1106.5	1115	1123.5	1132	1140.5	1149	1157.5	1166	1174.5	1183
20	1028	1036.5	1045	1053.5	1062	1070.5	1079	1087.5	1096	1104.5	1113	1121.5	1130	1138.5	1147	1155.5	1164	1172.5	1181	1189.5	1198	1206.5	1215	1223.5	1232
21	1077	1085.5	1094	1102.5	1111	1119.5	1128	1136.5	1145	1153.5	1162	1170.5	1179	1187.5	1196	1204.5	1213	1221.5	1230	1238.5	1247	1255.5	1264	1272.5	1281
22	1126	1134.5	1143	1151.5	1160	1168.5	1177	1185.5	1194	1202.5	1211	1219.5	1228	1236.5	1245	1253.5	1262	1270.5	1279	1287.5	1296	1304.5	1313	1321.5	1330
23	1175	1183.5	1192	1200.5	1209	1217.5	1226	1234.5	1243	1251.5	1260	1268.5	1277	1285.5	1294	1302.5	1311	1319.5	1328	1336.5	1345	1353.5	1362	1370.5	1379
24	1224	1232.5	1241	1249.5	1258	1266.5	1275	1283.5	1292	1300.5	1309	1317.5	1326	1334.5	1343	1351.5	1360	1368.5	1377	1385.5	1394	1402.5	1411	1419.5	1428
25	1273	1281.5	1290	1298.5	1307	1315.5	1324	1332.5	1341	1349.5	1358	1366.5	1375	1383.5	1392	1400.5	1409	1417.5	1426	1434.5	1443	1451.5	1460	1468.5	1477

For singly charged species, the first table entry (0,1) is a bisulfate anion, with m/z = 97. Each term going down adds 98 – the mass-to-charge ratio of sulfuric acid – and each term

going across adds 17 – the mass-to-charge ratio of ammonia. For doubly charged species, every term is halved. The first entry (0,1) is half the mass-to-charge ratio of two bisulfate anions – 97. Entries going across add 8.5, whereas entries going down add 49. From the mass spectra, we cannot tell the structure of the clusters, so it is very possible that the charge carrier for the doubly charged clusters is a sulfate anion, instead of two bisulfate anions. The only difference this makes to the chart is that all masses are shifted down one row, to one higher sulfuric acid addition (SI 4.10). All the masses we would expect if there were two bisulfate anions still would be present if the charge carrier is one sulfate anion.

All entries on the singly charged chart exist on the doubly charged chart. To ensure which charge the clusters were, their isotope patterns were compared to theoretical isotope patterns in mMass. An example can be seen in Figure 4.5.

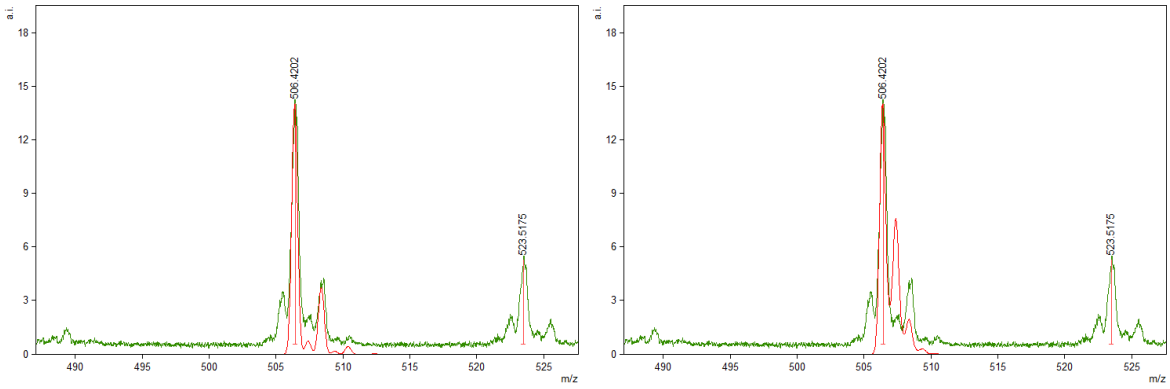

Figure 4.5 Isotope distribution fits. Since the masses for the singly charged clusters appear on both the singly and doubly charged charts, some peaks were fitted in mMass. Here, we see the peak at m/z = 506.4 fitted to the singly charged isotope distribution (left) and the doubly charged distribution (right). Based off this, the cluster at m/z = 506.4 is singly charged.

Table 4.3 Cluster compositions as seen on the LTQ. The solution used was 5 mM $(NH_4)_2SO_4$ in water/ 0.1% NH_4OH. Observed singly charged clusters are colored red; observed doubly charged masses are colored blue if the observed mass falls within m/z = 0.3 of the expected mass. They are lightly colored if the observed mass is between m/z = 0.4 to 0.8 of the expected mass. Clusters are colored purple if both singly and doubly charged clusters are observed for this combination.

	0	1	2	3	4	5	6	7	8	9	10	11	12	13	14	15	16	17	18	19	20	21	22	23	24
1	0,1	1,1	2,1	3,1	4,1	5,1	6,1	7,1	8,1	9,1	10,1	11,1	12,1	13,1	14,1	15,1	16,1	17,1	18,1	19,1	20,1	21,1	22,1	23,1	24,1
2	0,2	1,2	2,2	3,2	4,2	5,2	6,2	7,2	8,2	9,2	10,2	11,2	12,2	13,2	14,2	15,2	16,2	17,2	18,2	19,2	20,2	21,2	22,2	23,2	24,2
3	0,3	1,3	2,3	3,3	4,3	5,3	6,3	7,3	8,3	9,3	10,3	11,3	12,3	13,3	14,3	15,3	16,3	17,3	18,3	19,3	20,3	21,3	22,3	23,3	24,3
4	0,4	1,4	2,4	3,4	4,4	5,4	6,4	7,4	8,4	9,4	10,4	11,4	12,4	13,4	14,4	15,4	16,4	17,4	18,4	19,4	20,4	21,4	22,4	23,4	24,4
5	0,5	1,5	2,5	3,5	4,5	5,5	6,5	7,5	8,5	9,5	10,5	11,5	12,5	13,5	14,5	15,5	16,5	17,5	18,5	19,5	20,5	21,5	22,5	23,5	24,5
6	0,6	1,6	2,6	3,6	4,6	5,6	6,6	7,6	8,6	9,6	10,6	11,6	12,6	13,6	14,6	15,6	16,6	17,6	18,6	19,6	20,6	21,6	22,6	23,6	24,6
7	0,7	1,7	2,7	3,7	4,7	5,7	6,7	7,7	8,7	9,7	10,7	11,7	12,7	13,7	14,7	15,7	16,7	17,7	18,7	19,7	20,7	21,7	22,7	23,7	24,7
8	0,8	1,8	2,8	3,8	4,8	5,8	6,8	7,8	8,8	9,8	10,8	11,8	12,8	13,8	14,8	15,8	16,8	17,8	18,8	19,8	20,8	21,8	22,8	23,8	24,8
9	0,9	1,9	2,9	3,9	4,9	5,9	6,9	7,9	8,9	9,9	10,9	11,9	12,9	13,9	14,9	15,9	16,9	17,9	18,9	19,9	20,9	21,9	22,9	23,9	24,9
10	0,10	1,10	2,10	3,10	4,10	5,10	6,10	7,10	8,10	9,10	10,10	11,10	12,10	13,10	14,10	15,10	16,10	17,10	18,10	19,10	20,10	21,10	22,10	23,10	24,10
11	0,11	1,11	2,11	3,11	4,11	5,11	6,11	7,11	8,11	9,11	10,11	11,11	12,11	13,11	14,11	15,11	16,11	17,11	18,11	19,11	20,11	21,11	22,11	23,11	24,11
12	0,12	1,12	2,12	3,12	4,12	5,12	6,12	7,12	8,12	9,12	10,12	11,12	12,12	13,12	14,12	15,12	16,12	17,12	18,12	19,12	20,12	21,12	22,12	23,12	24,12
13	0,13	1,13	2,13	3,13	4,13	5,13	6,13	7,13	8,13	9,13	10,13	11,13	12,13	13,13	14,13	15,13	16,13	17,13	18,13	19,13	20,13	21,13	22,13	23,13	24,13
14	0,14	1,14	2,14	3,14	4,14	5,14	6,14	7,14	8,14	9,14	10,14	11,14	12,14	13,14	14,14	15,14	16,14	17,14	18,14	19,14	20,14	21,14	22,14	23,14	24,14
15	0,15	1,15	2,15	3,15	4,15	5,15	6,15	7,15	8,15	9,15	10,15	11,15	12,15	13,15	14,15	15,15	16,15	17,15	18,15	19,15	20,15	21,15	22,15	23,15	24,15
16	0,16	1,16	2,16	3,16	4,16	5,16	6,16	7,16	8,16	9,16	10,16	11,16	12,16	13,16	14,16	15,16	16,16	17,16	18,16	19,16	20,16	21,16	22,16	23,16	24,16
17	0,17	1,17	2,17	3,17	4,17	5,17	6,17	7,17	8,17	9,17	10,17	11,17	12,17	13,17	14,17	15,17	16,17	17,17	18,17	19,17	20,17	21,17	22,17	23,17	24,17
18	0,18	1,18	2,18	3,18	4,18	5,18	6,18	7,18	8,18	9,18	10,18	11,18	12,18	13,18	14,18	15,18	16,18	17,18	18,18	19,18	20,18	21,18	22,18	23,18	24,18
19	0,19	1,19	2,19	3,19	4,19	5,19	6,19	7,19	8,19	9,19	10,19	11,19	12,19	13,19	14,19	15,19	16,19	17,19	18,19	19,19	20,19	21,19	22,19	23,19	24,19
20	0,20	1,20	2,20	3,20	4,20	5,20	6,20	7,20	8,20	9,20	10,20	11,20	12,20	13,20	14,20	15,20	16,20	17,20	18,20	19,20	20,20	21,20	22,20	23,20	24,20
21	0,21	1,21	2,21	3,21	4,21	5,21	6,21	7,21	8,21	9,21	10,21	11,21	12,21	13,21	14,21	15,21	16,21	17,21	18,21	19,21	20,21	21,21	22,21	23,21	24,21
22	0,22	1,22	2,22	3,22	4,22	5,22	6,22	7,22	8,22	9,22	10,22	11,22	12,22	13,22	14,22	15,22	16,22	17,22	18,22	19,22	20,22	21,22	22,22	23,22	24,22
23	0,23	1,23	2,23	3,23	4,23	5,23	6,23	7,23	8,23	9,23	10,23	11,23	12,23	13,23	14,23	15,23	16,23	17,23	18,23	19,23	20,23	21,23	22,23	23,23	24,23
24	0,24	1,24	2,24	3,24	4,24	5,24	6,24	7,24	8,24	9,24	10,24	11,24	12,24	13,24	14,24	15,24	16,24	17,24	18,24	19,24	20,24	21,24	22,24	23,24	24,24
25	0,25	1,25	2,25	3,25	4,25	5,25	6,25	7,25	8,25	9,25	10,25	11,25	12,25	13,25	14,25	15,25	16,25	17,25	18,25	19,25	20,25	21,25	22,25	23,25	24,25

Table 4.4 Cluster compositions as seen on the TOF. The solution used was 50:50 5 mM $(NH_4)_2SO_4$ in water/ 0.1% NH_4OH:methanol. Observed singly charged masses are colored red; observed doubly charged masses are colored blue if the observed mass falls within m/z = 0.3 of the expected mass. They are lightly colored if the observed mass is between m/z = 0.4 to 0.8 of the expected mass.

	0	1	2	3	4	5	6	7	8	9	10	11	12	13	14	15	16	17	18	19	20	21	22	23	24
1	0,1	1,1	2,1	3,1	4,1	5,1	6,1	7,1	8,1	9,1	10,1	11,1	12,1	13,1	14,1	15,1	16,1	17,1	18,1	19,1	20,1	21,1	22,1	23,1	24,1
2	0,2	1,2	2,2	3,2	4,2	5,2	6,2	7,2	8,2	9,2	10,2	11,2	12,2	13,2	14,2	15,2	16,2	17,2	18,2	19,2	20,2	21,2	22,2	23,2	24,2
3	0,3	1,3	2,3	3,3	4,3	5,3	6,3	7,3	8,3	9,3	10,3	11,3	12,3	13,3	14,3	15,3	16,3	17,3	18,3	19,3	20,3	21,3	22,3	23,3	24,3
4	0,4	1,4	2,4	3,4	4,4	5,4	6,4	7,4	8,4	9,4	10,4	11,4	12,4	13,4	14,4	15,4	16,4	17,4	18,4	19,4	20,4	21,4	22,4	23,4	24,4
5	0,5	1,5	2,5	3,5	4,5	5,5	6,5	7,5	8,5	9,5	10,5	11,5	12,5	13,5	14,5	15,5	16,5	17,5	18,5	19,5	20,5	21,5	22,5	23,5	24,5
6	0,6	1,6	2,6	3,6	4,6	5,6	6,6	7,6	8,6	9,6	10,6	11,6	12,6	13,6	14,6	15,6	16,6	17,6	18,6	19,6	20,6	21,6	22,6	23,6	24,6
7	0,7	1,7	2,7	3,7	4,7	5,7	6,7	7,7	8,7	9,7	10,7	11,7	12,7	13,7	14,7	15,7	16,7	17,7	18,7	19,7	20,7	21,7	22,7	23,7	24,7
8	0,8	1,8	2,8	3,8	4,8	5,8	6,8	7,8	8,8	9,8	10,8	11,8	12,8	13,8	14,8	15,8	16,8	17,8	18,8	19,8	20,8	21,8	22,8	23,8	24,8
9	0,9	1,9	2,9	3,9	4,9	5,9	6,9	7,9	8,9	9,9	10,9	11,9	12,9	13,9	14,9	15,9	16,9	17,9	18,9	19,9	20,9	21,9	22,9	23,9	24,9
10	0,10	1,10	2,10	3,10	4,10	5,10	6,10	7,10	8,10	9,10	10,10	11,10	12,10	13,10	14,10	15,10	16,10	17,10	18,10	19,10	20,10	21,10	22,10	23,10	24,10
11	0,11	1,11	2,11	3,11	4,11	5,11	6,11	7,11	8,11	9,11	10,11	11,11	12,11	13,11	14,11	15,11	16,11	17,11	18,11	19,11	20,11	21,11	22,11	23,11	24,11
12	0,12	1,12	2,12	3,12	4,12	5,12	6,12	7,12	8,12	9,12	10,12	11,12	12,12	13,12	14,12	15,12	16,12	17,12	18,12	19,12	20,12	21,12	22,12	23,12	24,12
13	0,13	1,13	2,13	3,13	4,13	5,13	6,13	7,13	8,13	9,13	10,13	11,13	12,13	13,13	14,13	15,13	16,13	17,13	18,13	19,13	20,13	21,13	22,13	23,13	24,13
14	0,14	1,14	2,14	3,14	4,14	5,14	6,14	7,14	8,14	9,14	10,14	11,14	12,14	13,14	14,14	15,14	16,14	17,14	18,14	19,14	20,14	21,14	22,14	23,14	24,14
15	0,15	1,15	2,15	3,15	4,15	5,15	6,15	7,15	8,15	9,15	10,15	11,15	12,15	13,15	14,15	15,15	16,15	17,15	18,15	19,15	20,15	21,15	22,15	23,15	24,15
16	0,16	1,16	2,16	3,16	4,16	5,16	6,16	7,16	8,16	9,16	10,16	11,16	12,16	13,16	14,16	15,16	16,16	17,16	18,16	19,16	20,16	21,16	22,16	23,16	24,16
17	0,17	1,17	2,17	3,17	4,17	5,17	6,17	7,17	8,17	9,17	10,17	11,17	12,17	13,17	14,17	15,17	16,17	17,17	18,17	19,17	20,17	21,17	22,17	23,17	24,17
18	0,18	1,18	2,18	3,18	4,18	5,18	6,18	7,18	8,18	9,18	10,18	11,18	12,18	13,18	14,18	15,18	16,18	17,18	18,18	19,18	20,18	21,18	22,18	23,18	24,18
19	0,19	1,19	2,19	3,19	4,19	5,19	6,19	7,19	8,19	9,19	10,19	11,19	12,19	13,19	14,19	15,19	16,19	17,19	18,19	19,19	20,19	21,19	22,19	23,19	24,19
20	0,20	1,20	2,20	3,20	4,20	5,20	6,20	7,20	8,20	9,20	10,20	11,20	12,20	13,20	14,20	15,20	16,20	17,20	18,20	19,20	20,20	21,20	22,20	23,20	24,20
21	0,21	1,21	2,21	3,21	4,21	5,21	6,21	7,21	8,21	9,21	10,21	11,21	12,21	13,21	14,21	15,21	16,21	17,21	18,21	19,21	20,21	21,21	22,21	23,21	24,21
22	0,22	1,22	2,22	3,22	4,22	5,22	6,22	7,22	8,22	9,22	10,22	11,22	12,22	13,22	14,22	15,22	16,22	17,22	18,22	19,22	20,22	21,22	22,22	23,22	24,22
23	0,23	1,23	2,23	3,23	4,23	5,23	6,23	7,23	8,23	9,23	10,23	11,23	12,23	13,23	14,23	15,23	16,23	17,23	18,23	19,23	20,23	21,23	22,23	23,23	24,23
24	0,24	1,24	2,24	3,24	4,24	5,24	6,24	7,24	8,24	9,24	10,24	11,24	12,24	13,24	14,24	15,24	16,24	17,24	18,24	19,24	20,24	21,24	22,24	23,24	24,24
25	0,25	1,25	2,25	3,25	4,25	5,25	6,25	7,25	8,25	9,25	10,25	11,25	12,25	13,25	14,25	15,25	16,25	17,25	18,25	19,25	20,25	21,25	22,25	23,25	24,25

Singly charged clusters are represented in red if the observed mass falls within m/z = 0.3 of the nominal m/z, and pink if they are between m/z = 0.4 to 0.8. Doubly charged clusters are dark blue and light blue, respectively, for the same conditions. Clusters that occur

as both singly and doubly charged are marked in purple. Table 4.3 shows the marked chart for the mass spectrum from the LTQ, and Table 4.4 shows the marked chart from our TOF instrument.

The purple entries only exist because the charge carrier that the doubly charged table is based off of is two bisulfate ions. If the charge carrier used as the basis for the chart were a sulfate ion instead, all the blue entries would be shifted down one row. This would still lead to a continuous trend, but without overlapping entries.

The charts, especially the chart of the clusters formed on the LTQ, show that there is a pattern to these clusters. We have termed the imaginary line running diagonally down the chart at equal ammonia and sulfuric acid addition "the Line of Maximum Saltiness". As evident in the chart, and as previous experiments have indicated,[2] sulfuric acid adds to the clusters before ammonia does for anions. Then, as the clusters get larger and more ammonia is added, the clusters approach the line of maximum saltiness.

As with the cationic clusters, we also explored amine substitution with these anionic clusters. First, we wanted to see if we could push cluster formation towards the line of maximum saltiness sooner. We attempted this by introducing ammonia into the atmosphere via a capsule containing ammonium hydroxide attached to the electrospray region of the instrument.

This was able to be done, as shown in Figure 4.6 (Full mass spectrum in SI 4.11), but not for very long, and not for many peaks, as the ammonia in the atmosphere would be used very quickly and need to be replenished. In order for this to work well, there must be a continuous flow of ammonia into the atmosphere. Ammonia did not add onto clusters that did not already contain ammonia.

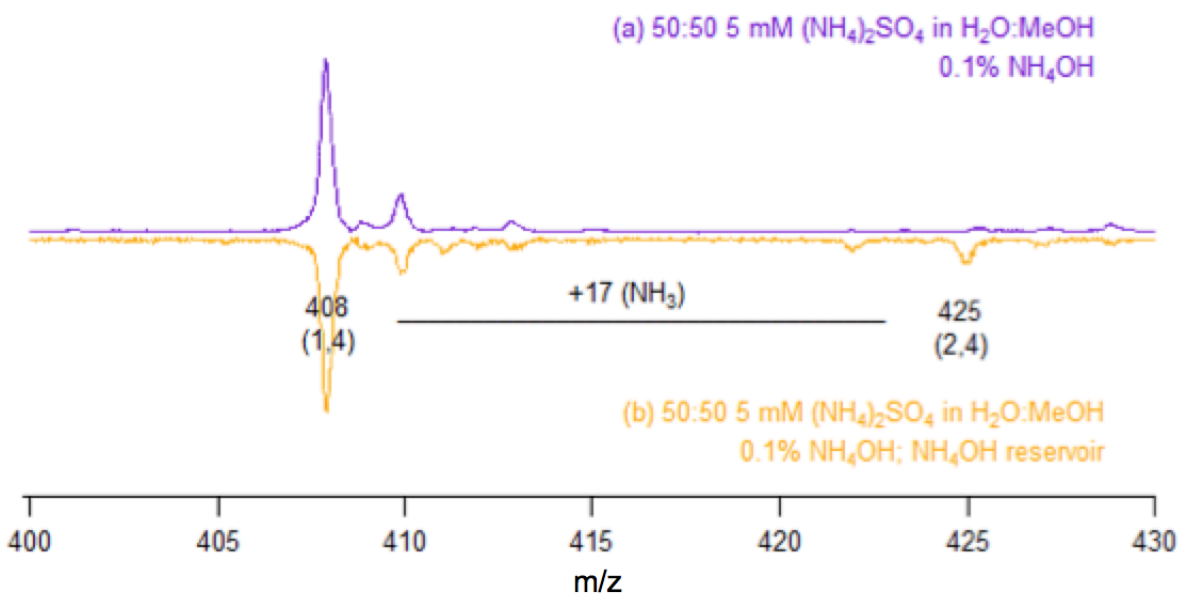

Figure 4.6 Partial mass spectrum for NH_3 addition. Here, we see a large peak at 408 (1,3) on both spectra, but 425 (2,3) only exists in the spectrum pertaining to conditions with the NH_4OH reservoir attached to the electrospray atmosphere.

Amine substitution was attempted by introducing dimethylamine and trimethylamine into the ESI atmosphere individually. Similarly to ammonia addition, the dimethylamine and trimethylamine substitutions were fleeting, and only occurred on a few clusters.

Dimethylamine (Figure 4.7, full mass spectrum in SI 4.12) added once and twice to the (0,3) cluster. The (0,4) and (1,4) peaks disappeared, which is indicative of full conversion to added/substituted species: a peak at m/z = 436 coincides with addition onto the (0,4) cluster, or substitution into (1,4). There is also a peak at m/z = 481 (not shown in Figure 4.7) that could coincide with double addition to (0,4) or addition and substitution into (1,4). Trimethylamine (Figure 4.8, full mass spectrum in SI 4.13) also showed addition onto (0,4) and substitution into (1,4).

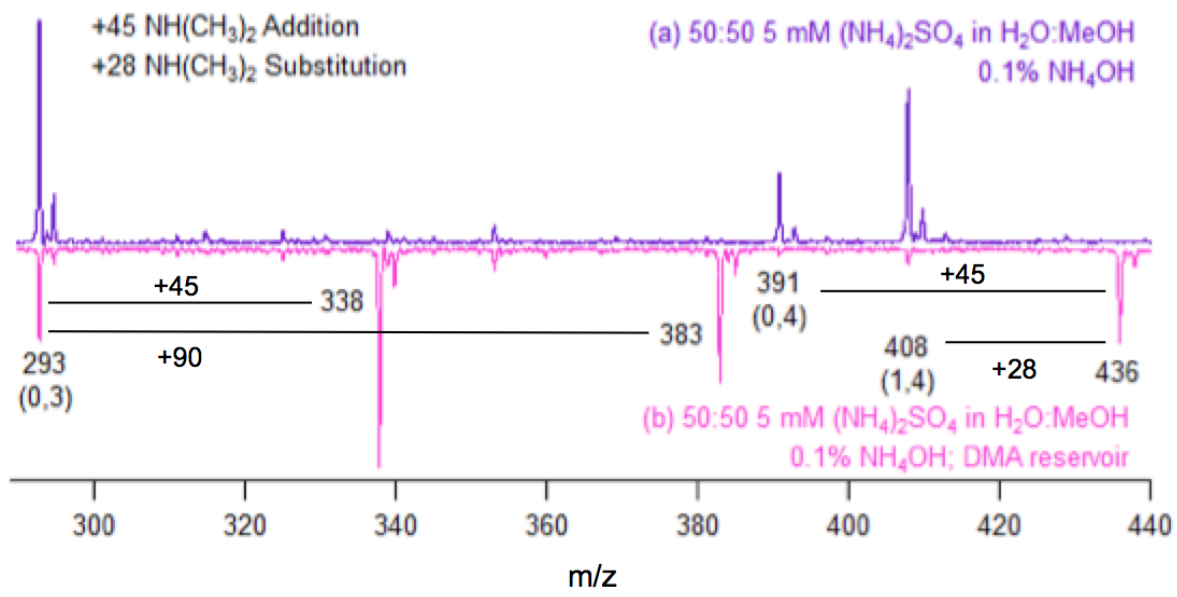

Figure 4.7 Partial mass spectrum for dimethylamine substitution. Dimethylamine was seen to add onto the (0,3) cluster. It was seen to also possibly add onto (0,4) or substitute onto (1,4).

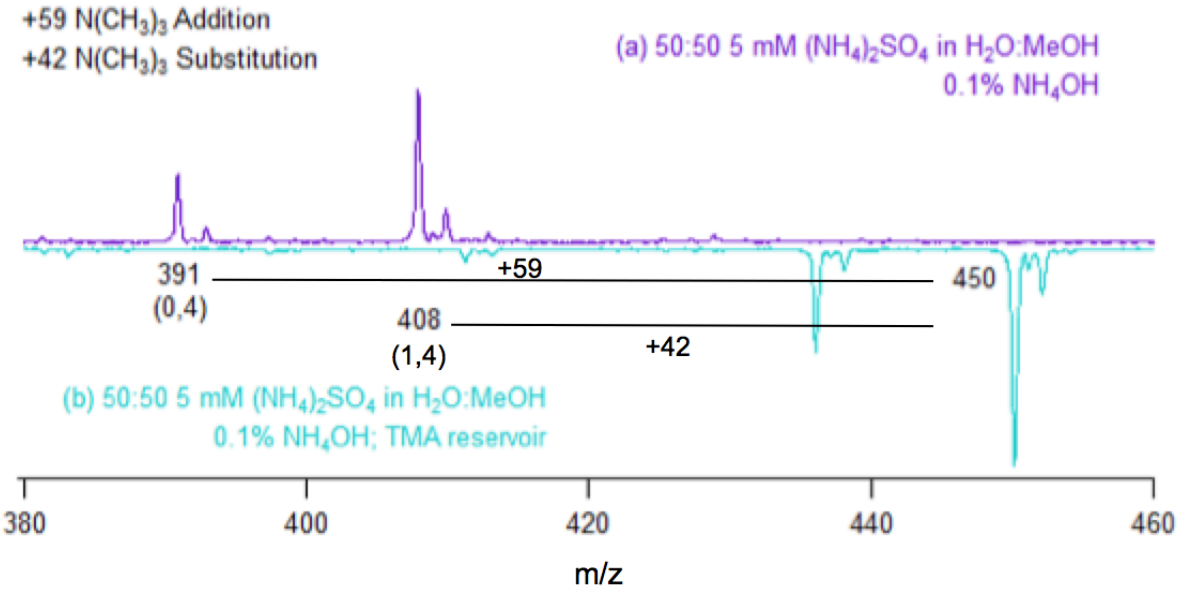

Figure 4.8 Partial mass spectrum for trimethylamine substitution. Trimethylamine was seen to add onto the (0,4) cluster and substitute into the (1,4) cluster.

We do not seem to see the same substitution patterns with the anionic clusters as we do the cationic clusters. In the future, we will need to work on getting a more stable environment for the amines, so that we can make better comparisons.

4.3 Future Work

First, we must determine whether the charge carrier for doubly charged ions is a sulfate or two bisulfates. This can be done two ways. If we can form enough of a doubly charged cluster, we can perform CID experiments to see how many of each species is present in the cluster. Alternatively, we can take infrared spectra of the clusters, which will have different symmetry based on the number of components present, and thus will show different spectra.

There exist multiply charged species in our mass spectra, especially in that from our TOF instrument, that have not been characterized for the work presented in this thesis.

For amine addition and substitution, the concentration of amines present in the electrospray environment's atmosphere must be increased and made more continuous. Once addition and substitution is more apparent and consistent, we can work on messenger tagging for CIVP to confirm the structures of these clusters.

References

1. Dunne, E. M.; et al. Global atmospheric particle formation from CERN CLOUD measurements. *Science*. [Online early access]. DOI: 10.1126/science.aaf2649. Published online 27 October 2016. http://science.sciencemag.org/content/early/2016/10/26/science.aaf2649 (accessed 3 April 2017).
2. Bianchi, F.; et al. Insight into Acid-base Nucleation Experiments by Comparison of the Chemical Composition of Positive, Negative, and Neutral Clusters. *Environ. Sci. Technol.* **2014**, *48*, 13675–13684.
3. Lehtipalo, K.; et al. The effect of acid-base clustering and ions on the growth of atmospheric nano-particles. *Nature Comm.* **2016**, *7*, 11594.
4. Spilä, M.; et al. The Role of Sulfuric Acid in Atmosheric Nucleation. *Science*. **2010**, *327*, 1243 – 1246.
5. Boucher, O.; et al. Clouds and Aerosols. *Climate Change 2013: The Physical Science Basis. Contribution of Working Group I to the Fifth Assessment Report of the Intergovernmental Panel on Climate Change.* **2013**, 596.
6. Kurtén, T.; Loukonen, V; Vehkamäki, H.; Kumala, M. Amines are likely to enhance neutral and ion-induced sulfuric acid-water nucleation in the atmosphere more effectively than ammonia. *Atmos. Chem. Phys.* **2008**, *8*, 4095 – 4103.
7. Yacovitch, T. I.; et al. Vibrational Spectroscopy of Bisulfate/Sulfuric Acid/Water Clusters: Structure, Stability, and Infrared Multiple-Photon Dissociation. *J. Phys. Chem. A*. **2013**, *117*, 7081 – 7090.

8. Strohalm, M.; Hassman, M.; Košata, B.; Kodíček, M. *mMass* data miner: an open source alternative for mass spectrometric data analysis. *Rapid Commun. Mass Spec.* **2008**, *22*, 905 – 908.

5. Supplemental Information

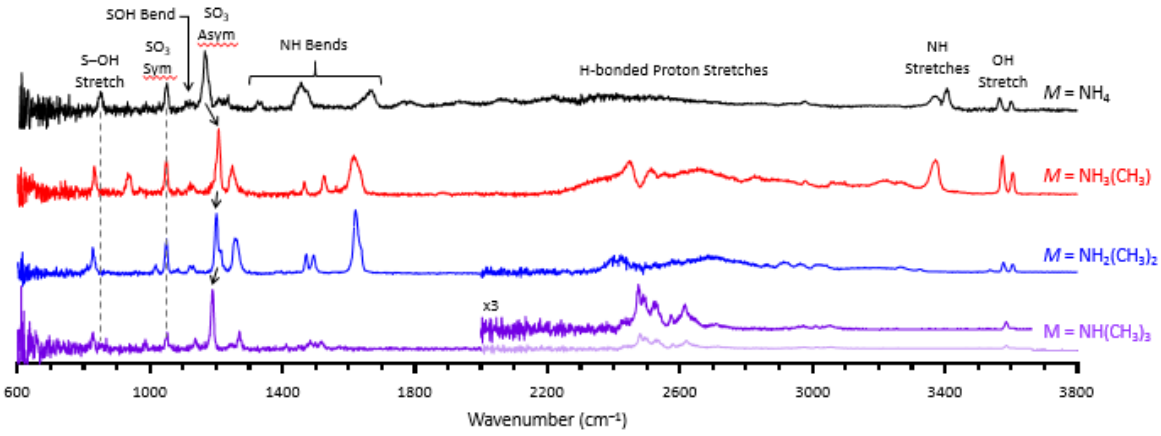

SI 4.1 IR spectra of (2,1) unsubstituted and fully substituted clusters.

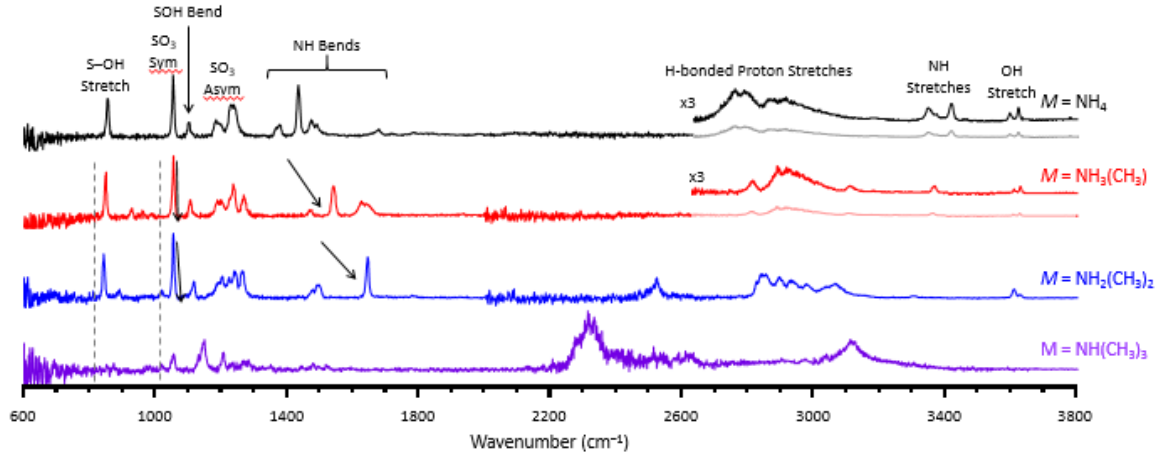

SI 4.2 IR spectra of (3,2) unsubstituted and fully substituted clusters.

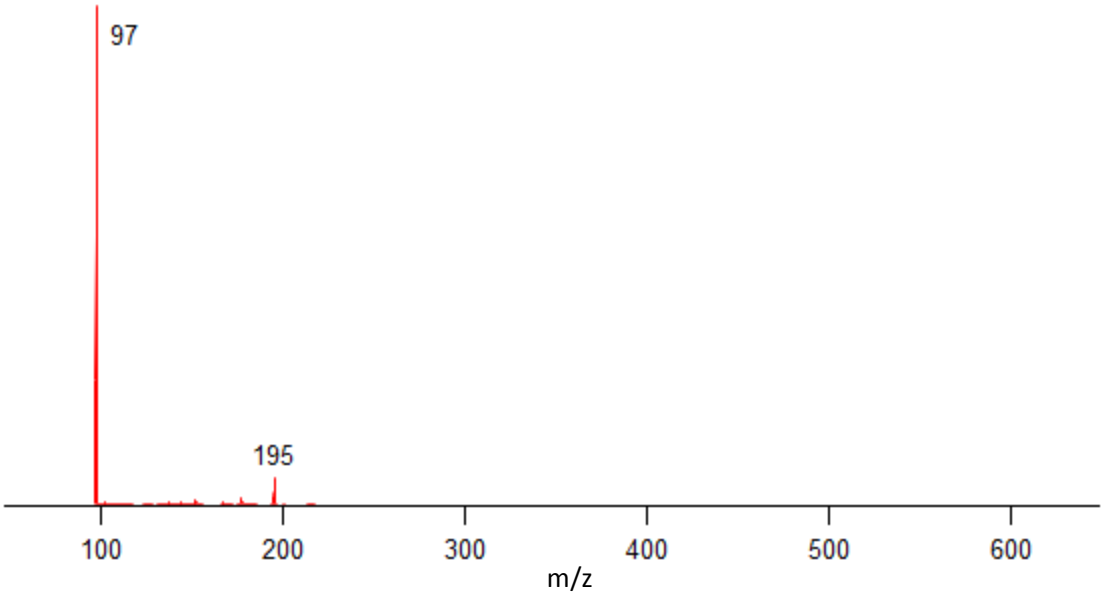

SI 4.3 CID spectrum of 195 (0,2). 195 fragments into 97 (0,1), which shows H_2SO_4 loss.

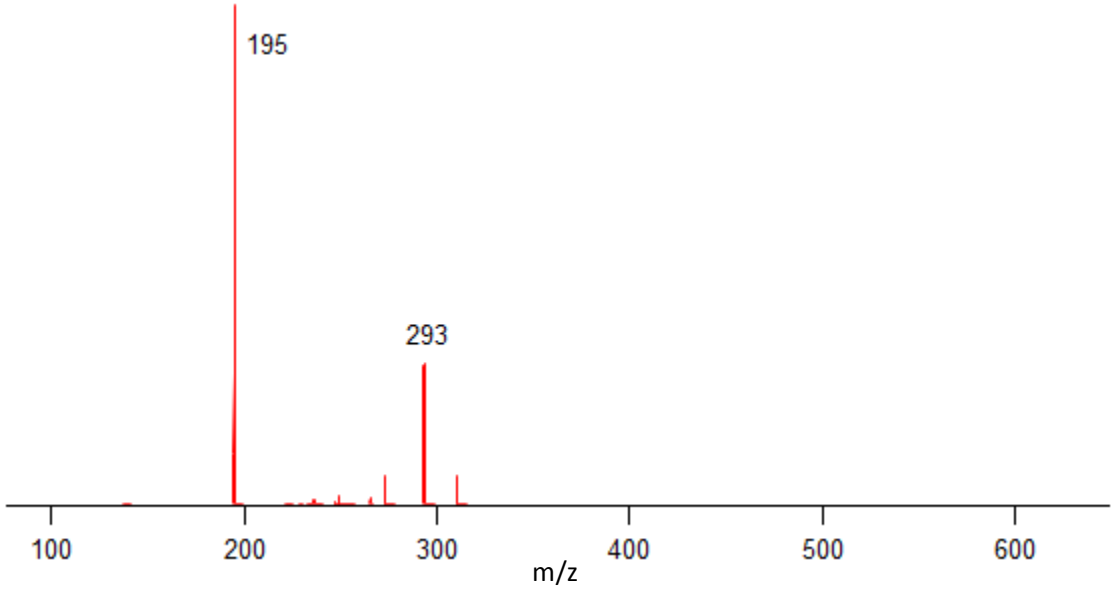

SI 4.4 CID spectrum of 293 (0,3). 293 fragments into 195 (0,2), which shows H_2SO_4 loss.

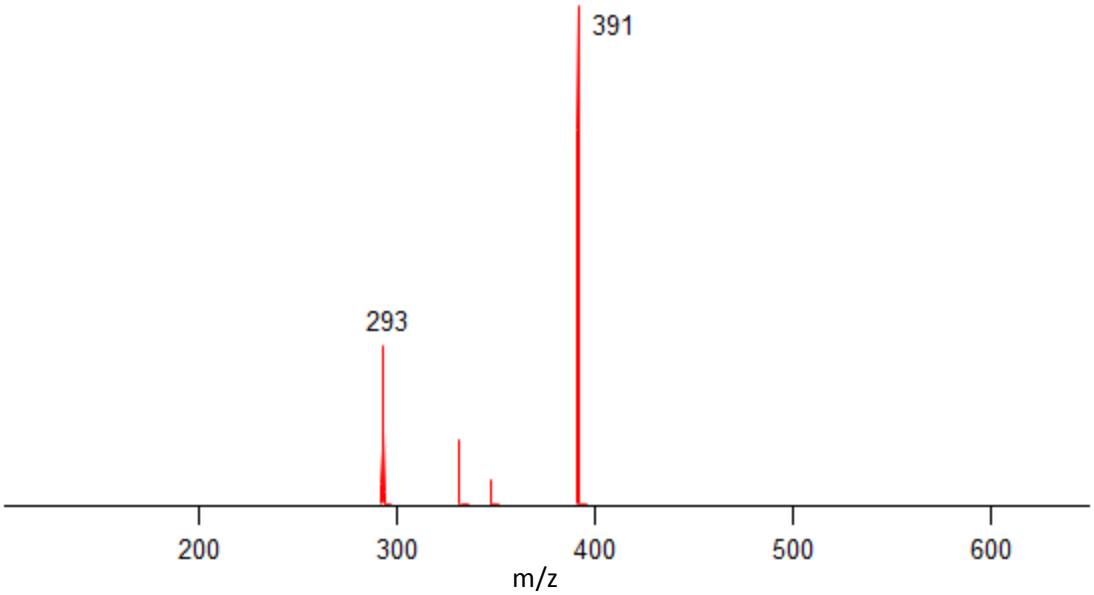

SI 4.5 CID spectrum of 391 (0,4). 391 fragments into 293 (0,3), which shows H_2SO_4 loss.

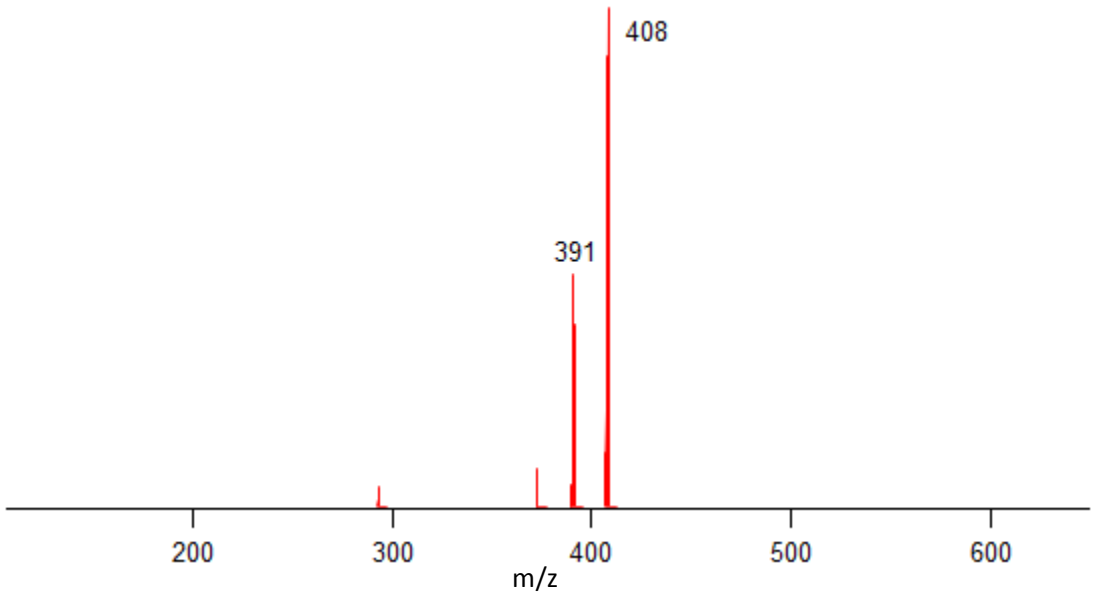

SI 4.6 CID spectrum of 408 (1,4). 408 fragments into 391 (0,4), which shows NH_3 loss.

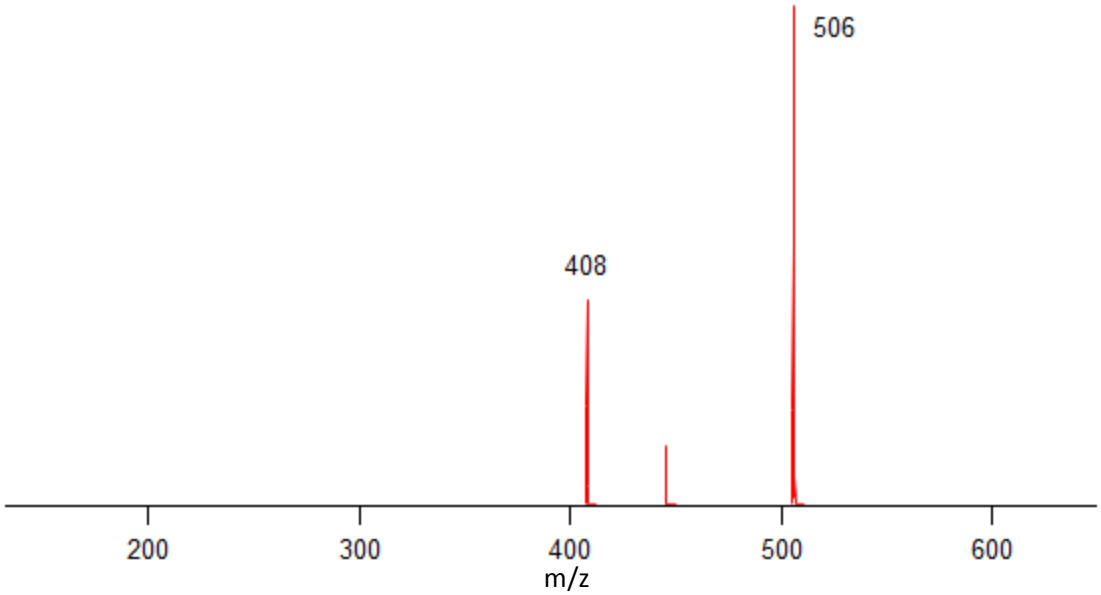

SI 4.7 CID spectrum of 506 (1,5). 506 fragments into 408 (1,4), which shows H_2SO_4 loss.

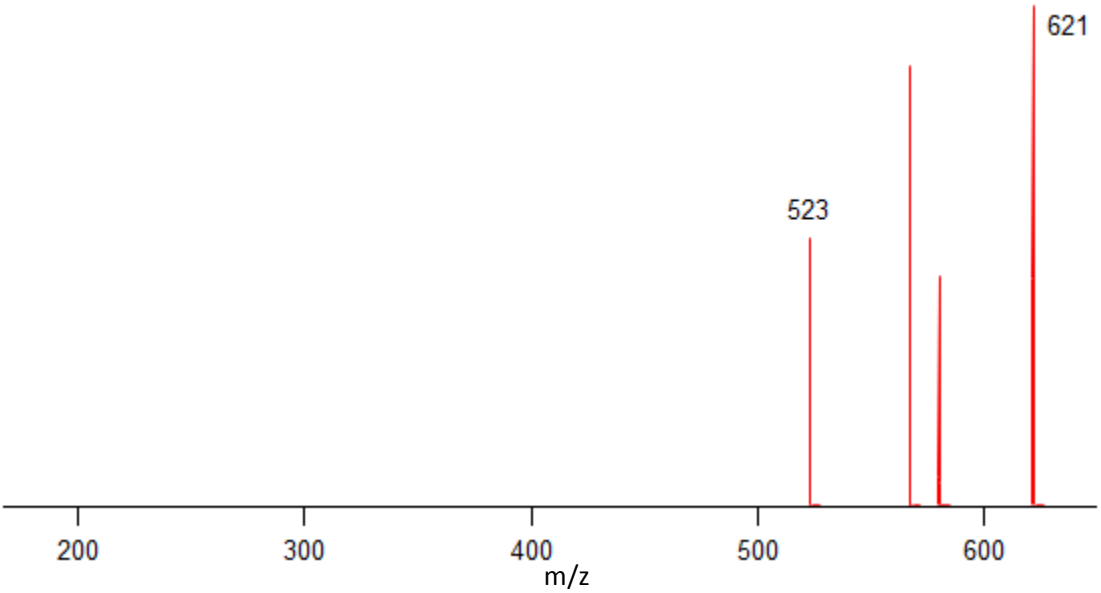

SI 4.8 CID spectrum of 621 (2,6). 621 fragments into 523 (2,5), which shows H_2SO_4 loss. There were very few m/z = 621 ions, so inaccuracies may appear.

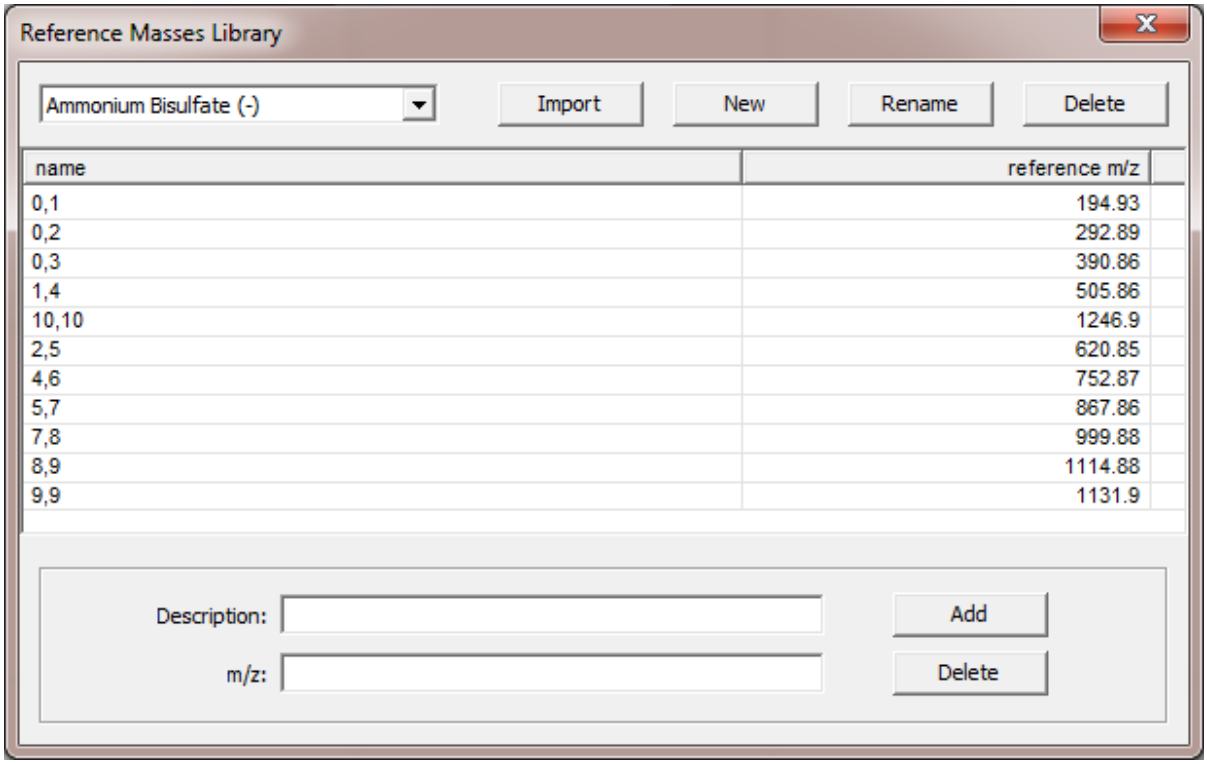

SI 4.9 mMass calibration reference library.

SI 4.10 Expected mass-to-charge ratio chart for doubly charged species. The first entry (0,1) represents the charge carrier for this chart: one sulfate anion. Across a row represents more ammonia addition; down a column represents more sulfuric acid addition. Every entry is divided by 2 for the mass-to-charge ratio of each cluster.

	0	1	2	3	4	5	6	7	8	9	10	11	12	13	14	15	16	17	18	19	20	21	22	23	24
1	48.5	57	65.5	74	82.5	91	99.5	108	116.5	125	133.5	142	150.5	159	167.5	176	184.5	193	201.5	210	218.5	227	235.5	244	252.5
2	97.5	106	114.5	123	131.5	140	148.5	157	165.5	174	182.5	191	199.5	208	216.5	225	233.5	242	250.5	259	267.5	276	284.5	293	301.5
3	146.5	155	163.5	172	180.5	189	197.5	206	214.5	223	231.5	240	248.5	257	265.5	274	282.5	291	299.5	308	316.5	325	333.5	342	350.5
4	195.5	204	212.5	221	229.5	238	246.5	255	263.5	272	280.5	289	297.5	306	314.5	323	331.5	340	348.5	357	365.5	374	382.5	391	399.5
5	244.5	253	261.5	270	278.5	287	295.5	304	312.5	321	329.5	338	346.5	355	363.5	372	380.5	389	397.5	406	414.5	423	431.5	440	448.5
6	293.5	302	310.5	319	327.5	336	344.5	353	361.5	370	378.5	387	395.5	404	412.5	421	429.5	438	446.5	455	463.5	472	480.5	489	497.5
7	342.5	351	359.5	368	376.5	385	393.5	402	410.5	419	427.5	436	444.5	453	461.5	470	478.5	487	495.5	504	512.5	521	529.5	538	546.5
8	391.5	400	408.5	417	425.5	434	442.5	451	459.5	468	476.5	485	493.5	502	510.5	519	527.5	536	544.5	553	561.5	570	578.5	587	595.5
9	440.5	449	457.5	466	474.5	483	491.5	500	508.5	517	525.5	534	542.5	551	559.5	568	576.5	585	593.5	602	610.5	619	627.5	636	644.5
10	489.5	498	506.5	515	523.5	532	540.5	549	557.5	566	574.5	583	591.5	600	608.5	617	625.5	634	642.5	651	659.5	668	676.5	685	693.5
11	538.5	547	555.5	564	572.5	581	589.5	598	606.5	615	623.5	632	640.5	649	657.5	666	674.5	683	691.5	700	708.5	717	725.5	734	742.5
12	587.5	596	604.5	613	621.5	630	638.5	647	655.5	664	672.5	681	689.5	698	706.5	715	723.5	732	740.5	749	757.5	766	774.5	783	791.5
13	636.5	645	653.5	662	670.5	679	687.5	696	704.5	713	721.5	730	738.5	747	755.5	764	772.5	781	789.5	798	806.5	815	823.5	832	840.5
14	685.5	694	702.5	711	719.5	728	736.5	745	753.5	762	770.5	779	787.5	796	804.5	813	821.5	830	838.5	847	855.5	864	872.5	881	889.5
15	734.5	743	751.5	760	768.5	777	785.5	794	802.5	811	819.5	828	836.5	845	853.5	862	870.5	879	887.5	896	904.5	913	921.5	930	938.5
16	783.5	792	800.5	809	817.5	826	834.5	843	851.5	860	868.5	877	885.5	894	902.5	911	919.5	928	936.5	945	953.5	962	970.5	979	987.5
17	832.5	841	849.5	858	866.5	875	883.5	892	900.5	909	917.5	926	934.5	943	951.5	960	968.5	977	985.5	994	1002.5	1011	1019.5	1028	1036.5
18	881.5	890	898.5	907	915.5	924	932.5	941	949.5	958	966.5	975	983.5	992	1000.5	1009	1017.5	1026	1034.5	1043	1051.5	1060	1068.5	1077	1085.5
19	930.5	939	947.5	956	964.5	973	981.5	990	998.5	1007	1015.5	1024	1032.5	1041	1049.5	1058	1066.5	1075	1083.5	1092	1100.5	1109	1117.5	1126	1134.5
20	979.5	988	996.5	1005	1013.5	1022	1030.5	1039	1047.5	1056	1064.5	1073	1081.5	1090	1098.5	1107	1115.5	1124	1132.5	1141	1149.5	1158	1166.5	1175	1183.5
21	1028.5	1037	1045.5	1054	1062.5	1071	1079.5	1088	1096.5	1105	1113.5	1122	1130.5	1139	1147.5	1156	1164.5	1173	1181.5	1190	1198.5	1207	1215.5	1224	1232.5
22	1077.5	1086	1094.5	1103	1111.5	1120	1128.5	1137	1145.5	1154	1162.5	1171	1179.5	1188	1196.5	1205	1213.5	1222	1230.5	1239	1247.5	1256	1264.5	1273	1281.5
23	1126.5	1135	1143.5	1152	1160.5	1169	1177.5	1186	1194.5	1203	1211.5	1220	1228.5	1237	1245.5	1254	1262.5	1271	1279.5	1288	1296.5	1305	1313.5	1322	1330.5
24	1175.5	1184	1192.5	1201	1209.5	1218	1226.5	1235	1243.5	1252	1260.5	1269	1277.5	1286	1294.5	1303	1311.5	1320	1328.5	1337	1345.5	1354	1362.5	1371	1379.5
25	1224.5	1233	1241.5	1250	1258.5	1267	1275.5	1284	1292.5	1301	1309.5	1318	1326.5	1335	1343.5	1352	1360.5	1369	1377.5	1386	1394.5	1403	1411.5	1420	1428.5

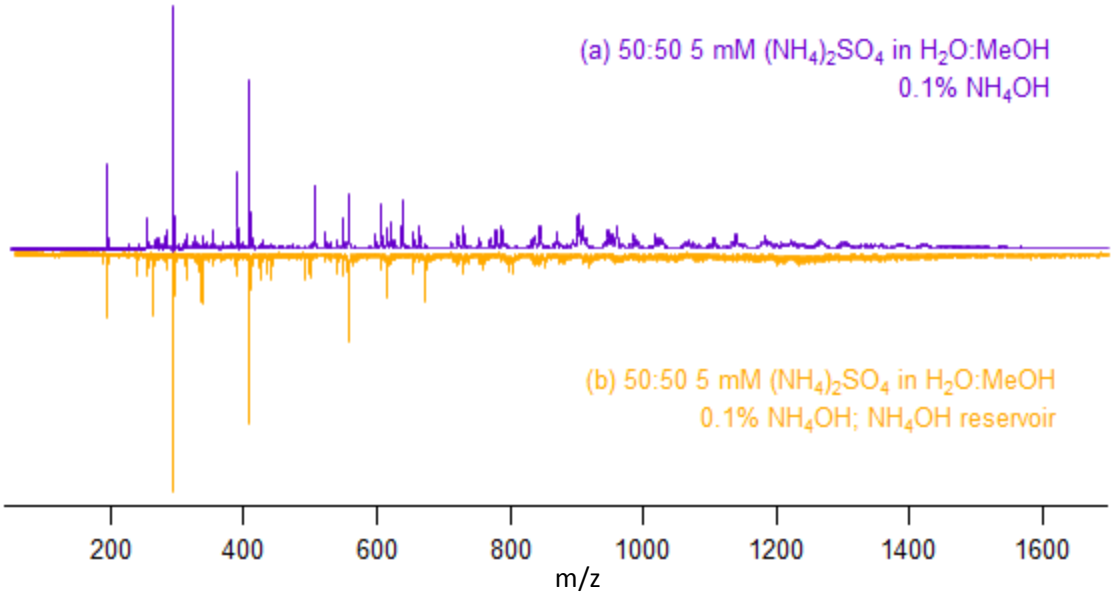

SI 4.11 Full mass spectrum for NH_3 addition.

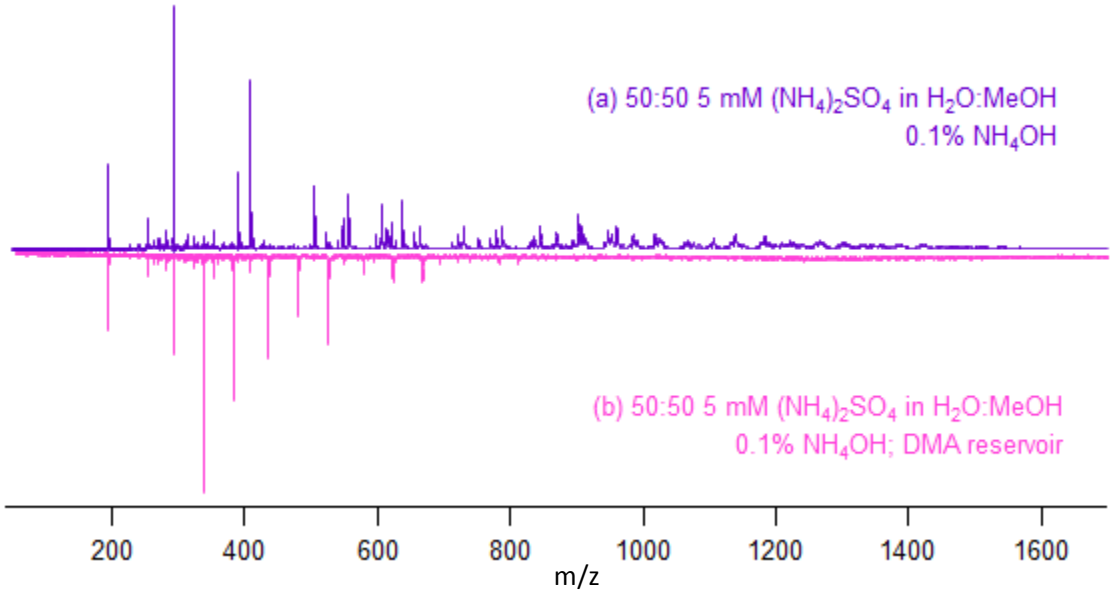

SI 4.12 Full mass spectrum for dimethylamine addition.

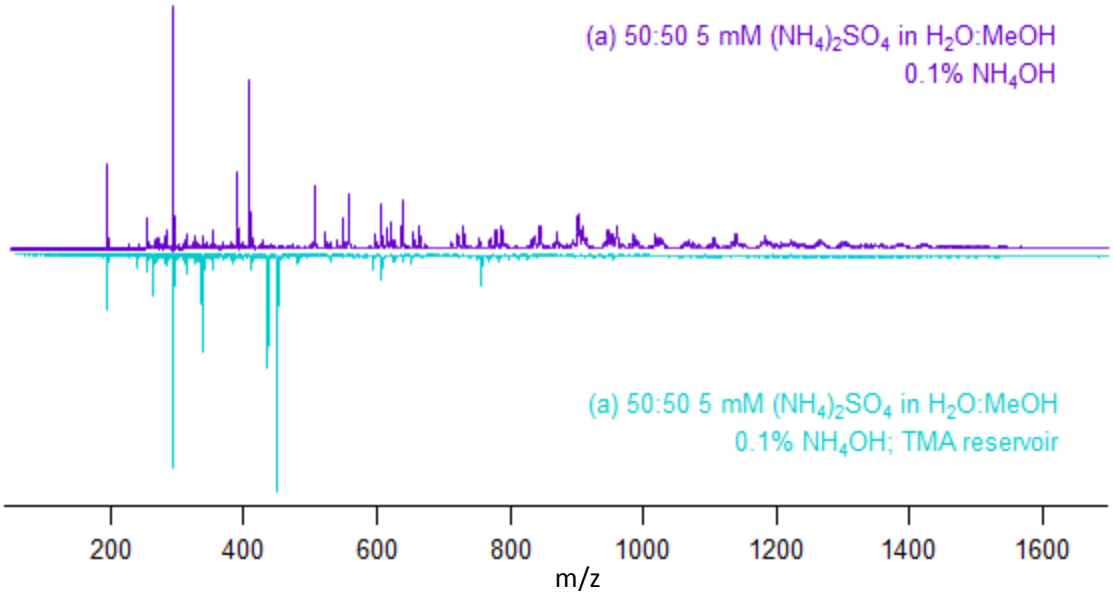

SI 4.13 Full mass spectrum for trimethylamine addition.